Journal of Biomolecular Structure and Dynamics

ISSN: 0739-1102 (Print) 1538-0254 (Online) Journal homepage: www.tandfonline.com/journals/tbsd20

Harnessing allosteric inhibition: prioritizing LIMK2 inhibitors for targeted cancer therapy through pharmacophore-based virtual screening and essential molecular dynamics

Raghu Rangaswamy, Nagarajan Hemavathy, Sneha Subramaniyan, Umashankar Vetrivel & Jeyaraman Jeyakanthan

To cite this article: Raghu Rangaswamy, Nagarajan Hemavathy, Sneha Subramaniyan, Umashankar Vetrivel & Jeyaraman Jeyakanthan (2025) Harnessing allosteric inhibition: prioritizing LIMK2 inhibitors for targeted cancer therapy through pharmacophore-based virtual screening and essential molecular dynamics, Journal of Biomolecular Structure and Dynamics, 43:3, 1129-1146, DOI: 10.1080/07391102.2023.2291171

To link to this article: https://doi.org/10.1080/07391102.2023.2291171

JOURNAL OF BIOMOLECULAR STRUCTURE AND DYNAMICS
2025, VOL. 43, NO. 3, 1129–1146
https://doi.org/10.1080/07391102.2023.2291171

Harnessing allosteric inhibition: prioritizing LIMK2 inhibitors for targeted cancer therapy through pharmacophore-based virtual screening and essential molecular dynamics

Raghu Rangaswamy[a], Nagarajan Hemavathy[a], Sneha Subramaniyan[a], Umashankar Vetrivel[b] and Jeyaraman Jeyakanthan[a]

[a]Structural Biology and Bio-Computing Lab, Department of Bioinformatics, Alagappa University, Karaikudi, Tamil Nadu, India; [b]Virology & Biotechnology/Bioinformatics Division, ICMR-National Institute for Research in Tuberculosis, Chennai, Tamil Nadu, India

ABSTRACT

The therapeutic potential of small molecule kinase inhibitors in cancer treatment is well recognized. However, achieving selectivity remains a formidable challenge, primarily due to the structural similarity of ATP binding pockets among kinases. Allosteric inhibition, which involves targeting binding pockets beyond the ATP-binding site, provides a promising alternative to overcome this challenge. In this study, a meticulous approach was implemented to prioritize type 3 inhibitors for LIMK2, employing a range of techniques including Molecular Dynamics (MD) simulations, e-pharmacophore-guided High Throughput Virtual Screening (HTVS), MM/GBSA and ADMETox analyses, Density Functional Theory (DFT) calculations, and MM/PBSA investigations. The e-pharmacophore model identifies a hypothesis featuring five essential pharmacophoric elements (RRRAH). Through virtual screening of the ZINC compound database, we identified only five compounds that align with all four pharmacophoric features: ZINC1044382792, ZINC1433610865, ZINC1044109145, ZINC952869440, and ZINC490621334. These compounds not only exhibit higher binding affinity but also demonstrate favorable ADME/Tox profiles. Molecular dynamics simulations underscore the stability of hydrogen bond interactions with critical cryptic LIMK2 pocket residues, Asp469 and Arg474, only for two compounds: ZINC143361086 and ZINC1044382792. These compounds also exhibit superior occupancy interactions, as indicated by HOMO-LUMO analysis. Additionally, binding free energy calculations highlight the significant affinities of these two compounds when complexed with LIMK2: −83.491 ± 1.230 kJ/mol and −90.122 ± 1.248 kJ/mol for ZINC1044382792 and ZINC1433610862, respectively. Hence, this comprehensive investigation identifies ZINC1433610862 and ZINC1044382792 as prospective hits, representing promising leads for targeting LIMK2 in cancer therapeutics.

ARTICLE HISTORY
Received 10 August 2023
Accepted 21 November 2023

KEYWORDS
LIMK2; Type 3 inhibitor; pharmacophore screening; molecular dynamics simulation

Introduction

LIM kinases (LIMKs) are the essential regulators for the cell cytoskeleton, which plays a major role in the development of various neurological disorders and also in the progression and spread of cancer. There are two homologs in the family of LIMK, including LIMK1 and LIMK2. Both are distinguishable in terms of expression profile, function, and intracellular localization. The core substrate of the LIMK is cofilin, which is a member of a family of actin-depolymerizing factor (ADF) proteins. The regulation of the actin cytoskeleton is carried out by LIM-kinases, which achieves this by phosphorylating cofilin at Ser3, as well as the substrates for Cdc42/Rac-PAK (Morales-Quinones et al., 2020; Sumi et al., 1999). This phosphorylation hinders the activity of cofilin, resulting in reduced depolymerization of actin filaments and thereby stabilizing it. LIM-kinase plays a role in a signal transduction pathway that facilitates the transmission of environmental signals *via* small GTPases of the Rho family through a protein kinase cascade (Maekawa et al., 1999). This pathway plays a crucial role in governing actin cytoskeleton responses, including cell movement, establishing the intracellular cytoplasmic organization, cell polarity, and various other functions that are vital for maintaining cellular homeostasis and ensuring survival. The regulation of cell progression can be influenced by the translocation of LIMKs into the nucleus. LIMKs possess a distinct feature, making them promising candidates for therapeutic targeting in tumors that lack merlin, like NF2.

The LIM kinases are involved in various cellular functions and also over-expressed in various types of cancers, however, the mechanism remains unclear. Recent studies have discovered that LIMK modulates the activity of the development of cancer, including cell proliferation, survival, and viability. The LIM domains exhibit auto-inhibition of the kinase domain of the proteins, which become activated *via* phosphorylation. Although LIMK1 is linked to the spread of cancer, LIMK2 activation facilitates advancement through the cell cycle. LIM

CONTACT Jeyaraman Jeyakanthan jjbioinformatics@gmail.com Structural Biology and Bio-Computing Lab, Department of Bioinformatics, Science Block, Alagappa University, Karaikudi, Tamil Nadu 630 003, India.

Supplemental data for this article can be accessed online at https://doi.org/10.1080/07391102.2023.2291171.

Domain Kinase 2 (LIMK2) serine/threonine kinase plays a crucial role in actin filament dynamics regulation due to its over-expression, growth, and invasion of numerous malignant tumors, including bladder cancer, osteosarcoma, glioblastoma, pancreatic cancer, lung cancer, and Triple Negative Breast cancer (Su et al., 2017, 2019, 2022). Furthermore, certain studies have also suggested that the expression and activity of LIMK2 increase following treatment with anticancer drugs, which has led to the implication of LIMK2 in drug resistance (Croft et al., 2011). Previous studies suggest that the expression of LIMK2 is also associated with deprived prognosis in many cancers. Due to the unclear mechanisms underlying LIMK-related tumorigenesis, there is a need to analyze the tumorigenic effects of LIM kinase 2 (LIMK2) in human cancers (Sooreshjani et al., 2021). Additionally, recent investigations have revealed that LIMK2 3′-UTR SNP rs2073859 (G-to-A allele) is associated with clinical features (Wang et al., 2019). Although the research focuses on various targets to combat malignant tumors, LIMK is a highly prominent target for many human cancers (Berabez et al., 2022; Manetti, 2012; Yoshioka et al., 2003). To date, only a few substrates are known for LIMK, and it will act as a potential tumor suppressor for human cancer and also can be used to understand the molecular mechanism. Lately, there has been much attention focused on creating pharmacological kinase inhibitors to address many cancers. Moreover, the advancement of a broad range of synthetic small-molecule kinase inhibitors has influenced the available treatment options (Zhang et al., 2009). The majority of the developed molecules fall under the category of LIMK type I inhibitors, which aim to inhibit the ATP-binding site in its active conformation (Fasano et al., 2014). Due to the significant similarity in the sequence of the ATP-binding site among the various kinase families, there is often reduced selectivity and an increased risk of toxicity when using kinase inhibitors. As a result, drug development strategists are exploring alternative approaches that target sites outside of the ATP cleft. One such approach involves Type III or allosteric inhibitors, which bind to site beyond the ATP-binding site and have demonstrated the ability to inhibit kinase activity.

There are various inhibitors available for kinases which are divided into three classes Type I, Type II, and Type III inhibitors. Type I inhibitors work by binding to the ATP-binding pocket and competing with the adenine component of ATP for crucial hydrogen-bonded interactions located in the 'hinge region'. Type II inhibitors were first identified with the detection of imatinib (Zhao et al., 2014). The Type II inhibitors bind not only to the ATP-binding pocket but also to a hydrophobic, allosteric pocket that is formed when the Asp-Phe-Gly (DFG) residues of the activation loop move away from their normal position ('DFG-out') and stabilize an inactive conformation of the kinase (Blanc et al., 2013; Richters et al., 2014). Moreover, a few Type III inhibitors also have been identified recently (Dasari et al., 2021; Fasano et al., 2014; Goodwin et al., 2015; Heymach et al., 2022). They bind to the kinase's catalytic domain, which is close to the ATP-binding pocket but without interacting with the hinge region. This type of inhibitor encompasses molecules that attach to the hydrophobic pocket generated by the DFG-out conformation (Okaniwa et al., 2012). The first Type III allosteric inhibitor reported for LIMK2, is a set of compounds that possess both N-phenyl sulfonamide and tertiary amide moieties that demonstrated exceptional potency against LIMK2 and remarkable selectivity against a range of other kinases. The Type III kinase inhibitors, referred to as allosteric inhibitors, bind to a location outside the ATP-binding site and exert to reduce the activity of the kinase. This group of inhibitors takes advantage of the allosteric characteristics of kinases. Allosteric refers to the holistic redistribution of protein conformational ensembles, resulting in various dynamic and functional effects. To overcome the current challenges associated with kinase inhibitors, such as poor selectivity and the emergence of drug resistance, targeting allosteric pockets outside of the highly conserved ATP pocket of kinases has been considered a promising alternative approach.

Small molecule kinase inhibitors have significant value as targeted therapeutics in the treatment of various human diseases, with a particular emphasis on their effectiveness in treating cancer (Wu, Nielsen, & Clausen, 2015b). Although the majority of preclinical small molecule inhibitors that have been developed and approved to target the ATP-binding pocket of kinases are classified as either Type I or Type II inhibitors, the high level of sequential and structural similarity among ATP pockets poses a significant challenge for achieving selective kinase inhibition (Wu, Clausen, & Nielsen, 2015a; Wu, Nielsen, & Clausen, 2015b). Recent investigations discuss the current understanding of allosteric inhibition, including its conceptual framework, classification, potential benefits, and contentious issues in the area (Wu, Clausen, & Nielsen, 2015a). In 2020, the US FDA approved four small molecule protein kinase antagonists: entrectinib, erdafitinib, pexidartinib, and fedratinib (Roskoski, 2020). By the year 2022, around two dozen distinct protein kinases were targeted by 62 FDA approved therapeutic agents (Roskoski, 2021). As of 2023, 72 FDA approved therapeutic agents target around two dozen distinct protein kinases, and in 2022, three of these drugs received approval (Roskoski, 2023). Even though the kinase and allosteric inhibitors have vast pharmacological properties, lipophilic efficiency, and ligand efficiency, the issue is further complicated by the likelihood of some allosteric pockets being involved in protein-protein and protein-peptide interactions, also bringing about conformational changes leading to drug resistance. In the context of cancer therapy, the potential benefits of incorporating allosteric inhibitors outweigh the associated risks. TKIs (Tyrosine Kinase Inhibitors) are known to cause dose-dependent adverse effects, and each drug has a unique broad side effect profile. However, due to similarities in drug targets, different classes of TKIs may exhibit similar side effect profiles (Jiao et al., 2018; Roskoski, 2023). One of the most significant issues with both targeted and cytotoxic drugs used in the treatment of cancer is the development of resistance to all therapeutic modalities. Therefore, it is reasonable to anticipate that combining various types of kinase inhibitors, such as ATP-competitive inhibitors, allosteric

inhibitors, and covalent inhibitors, could result in holistic kinase suppression and thereby lead to beneficial anticancer effects in clinical oncology settings.

Materials and methodology

Molecular modelling and molecular dynamics simulation

Among the available LIMK2 crystal structures, PDB ID: 5NXD (Mathea et al., 2017), LIMK2 co-crystallized with Type III inhibitor was considered as it was more relevant for this study. Since the structure had missing residues, E478-N509, appending the XDFG and Activation loop (Fig. S1a supplementary material), remodeling and refinement were performed using MODELLER10v (Eswar et al., 2006). From the generated models, the one with the least DOPE score was considered the best model and was subjected to a stereochemistry check by the Ramachandran plot using PROCHECK (Laskowski et al., 1993). The highly plausible model was further validated for structural stability using molecular dynamics simulation studies. The initial preprocessing steps for molecular dynamics (*apo* and other complexes) were performed using the CHARMM-GUI server (Jo et al., 2008) with CHARMM36m (Huang et al., 2017) as the force field. Wherein, the bonded constraints were handled with the LINCS algorithm (Hess et al., 1997), and the V-rescale weak coupling method was used for NVT equilibration at a constant temperature of 300K (Berendsen et al., 1984) for the system. In the case of NPT equilibration (at 1 atm), the Parrinello–Rahman method was incorporated into the system. The resultant equilibrated system was subjected to 200 ns MD simulation using the GROMACS2020v package, wherein the structural conformations were sampled at every 2 ps. Furthermore, the resulting MD trajectory was analyzed further for Root Mean Square Deviation (RMSD) of the protein backbone, and Root Mean Square Fluctuations (RMSF) of the residues during the production run. Moreover, essential molecular dynamics simulations such as PCA and FEL analysis (Maisuradze et al., 2009) were also performed to probe the near-native conformations of the complex and were considered for further studies.

Pharmacophore modelling

The pharmacophore approach involves identifying the specific molecular features required for a molecule to bind to a particular receptor which can be utilized as a guiding factor to perform virtual screening of vast compound libraries for the precise selection of the most promising candidates. The attempted structure-based method utilized the pharmacophore models of the ligands to establish the geometric constraints and type of chemical features. The PHASE (Pharmacophore Alignment and Scoring Engine) module of the Schrödinger suite was implemented to generate the pharmacophoric site, and based on the documented process of ranking and quantification, the final hypotheses were prioritized (Dixon, Smondyrev, & Rao, 2006). To rank the pharmacophoric hypotheses, common pharmacophoric features such as hydrogen bond acceptor (A), hydrogen bond donor (D), hydrophobic region (H), positive ionizable (P), negative ionizable (N), and aromatic ring (R) were used (Dixon, Smondyrev, Knoll et al., 2006). In this study, the near-native conformation of the LIMK-TH300 complex as predicted by MD was considered for pharmacophore feature generation, wherein the maximum number of features per hypothesis was set to 4-5, and other parameters were set to default values in the PHASE module. In the final hypotheses, sites that contribute to less than half of the heavy atoms in the pharmacophoric features were excluded. Finally, screening was carried out for the ZINC database 383,598,054 lead-like compounds against the generated and validated Hypothesis to generate the PhaseDB. Among the 383,598,054 compounds, the compounds that satisfy the hypothesis model with at least 4 pharmacophoric sites were shortlisted. Additionally, the compounds were sorted according to their fitness score, and the ligand conformer that best matched the hypotheses was aligned using vector matching and RMSD site evaluation. Subsequently, the generated dataset was considered for further High throughput virtual screening (HTVS) against LIMK2 (a grid box generated around the TH300 interacting residues) using the Glide module (Friesner et al., 2004). A stepwise structure-based virtual screening (SBVS) approach such as HTVS standard precision (SP) and extra precision (XP) docking was implemented to identify the potential lead molecule against LIMK2 (Friesner et al., 2006). Initially, the compounds were subjected to HTVS mode (50%), then the surpassed compounds from HTVS were further submitted to the SP (30%). Finally, from the 100% of hits that passed the XP docking [Glide (version 6.2). New York, NY: Schrodinger, LLC (2014)], based on the glide score, and glide energy, the top hits were shortlisted and were proceeded for drug likeliness and ADME prediction.

ADME/Tox prediction

The Qikprop module was utilized to predict the pharmacological properties of the identified compounds. QikProp is a software tool that swiftly and precisely forecasts crucial characteristics such as absorption, distribution, metabolism, excretion, and pharmaceutical properties of organic molecules/chemical compounds (Duffy & Jorgensen, 2000; Jorgensen & Duffy, 2002). It offers user-friendly functionality for predicting meaningful descriptors and relevant properties. Furthermore, QikProp generates a range of values that can be used to compare specific properties of a molecule with those of 95% of known drugs. It also identifies 30 types of reactive functional groups that could potentially produce false positive results in high throughput screening assays. The physicochemical characteristics of the molecules were thoroughly evaluated, including their Molecular Weight (MW), octanol/water partition coefficient (QPlogPo/w), aqueous solubility (QPlogS), skin permeability (QPlogKp), percentage of human oral absorption, and the descriptor values that fall outside the 95% range of similar values for known drugs. QikProp also assesses the suitability of the hit molecules by

applying Lipinski's rule of five, which is a significant factor in pharmacokinetics and rational drug design. Also, all the top-ranked compounds were further subjected to the SwissADME to validate the drug-likeness, ClogP, solubility, tumorigenic, TPSA, mutagenic effects, and other pharmacokinetic properties (Bakchi et al., 2022 Daina et al., 2017; Riyadi et al., 2021).

MM/GBSA analysis

The Molecular Mechanics Generalized Born and Solvent Accessibility (MM/GBSA) (Tuccinardi, 2021) method was employed to examine the binding affinities and strain energies of the foremost five lead compounds with the protein. The OPLS-AA force field was utilized to compute the ligand binding affinity within the active site residues, employing the solvation model for both polar solvation (SGB) and non-polar solvation (GNP). Furthermore, the intrinsic steric energy of the ligand and the intermolecular interactions within the protein-ligand complexes were computed through the assessment of binding energy. The alterations in binding free energy (ΔG) for the bound ligand within the LIMK binding pocket were determined using the following expression.

$$G = \Delta E_{MM} + \Delta G_{SGB} + \Delta G_{SA}$$

where, the term ΔE_{MM} represents the gas phase molecular mechanics (MM) energy, and the solvent generalized Born (GB) model was applied to compute the surface generalized Born (SGB) energy utilizing the default parameters. The change in solvation free energy (ΔG_{SA} SASA) was computed using the Linear Combinations of Pairwise Overlap (LCPO) method, where $G_{protein}$, G_{ligand}, and $G_{complex}$ represent the minimized solvation energies of the protein, ligand, and the protein-ligand complex, respectively (Genheden & Ryde, 2015).

Density functional theory

The DFT approach is a computational quantum mechanics (QM) method used to study the electronic structure of many-body systems, including atoms, molecules, and condensed phases. For the DFT calculations, the Jaguar module of the Schrödinger suite was employed to examine the energetic and geometrical properties of the potential top drug-like compounds (Bochevarov et al., 2013). The calculations utilized the B3LYP-D3 exchange potential (Becke's three-parameter exchange potential) and the Lee-Yang-Parr correlation hybrid function, with a basis set of 6–31 G^{*++} level (Lehtola et al., 2021). The Highest Occupied Molecular Orbital (HOMO) is directly linked to the ionization potential and acts as a nucleophile. The Lowest Unoccupied Molecular Orbital (LUMO) is associated with electron affinity and acts as an electrophile. The reactivity and stability of the ligands in this study were assessed by calculating the energy gaps and the distribution and energies of the HOMO and LUMO orbitals (Noureddine et al., 2021; Shahab et al., 2021).

MM/PBSA

MM/PBSA is an integrated molecular dynamics simulation technique employed to calculate the binding free energy within the specific active site between a protein and a ligand. The analysis of Gibbs's free energy calculations was performed using the g_mmpbsa.py script, which is integrated with the Gromacs. Further, the analysis was conducted for every 200 frames of the MD simulation to calculate the binding free energy of the complexes. The equation provided below can be used to calculate the binding free energy for biological complexes.

$$\Delta G_{bind} = \Delta G_{complex} - \left(\Delta G_{protein} + \Delta G_{ligand}\right)$$

The binding affinity, represented as ΔG_{bind}, is determined by the sum of the free energies of the biological complexes, which include $\Delta G_{protein}$ (free energy of the protein), $\Delta G_{ligands}$ (free energy of the ligands), and $\Delta G_{complex}$ (total free energy of the complex) (Botello-Smith & Luo, 2015; Kumari et al., 2014; Wang et al., 2017).

Results and discussion

Molecular modelling and molecular dynamics simulation

Since there was a missing segment (E478-N509) following the XDFG and Activation loop in the LIMK2-TH300 complex (PDB ID: 5NXD) (Figure.S1a, supplementary material), the structure was remodeled (Figure S1b, supplementary material). Further on refinement, the remodelled and refined LIMK2-TH300 complex (Figure 1) structure showed 92.7% in the most favored region with no residues in the disallowed region of the Ramachandran plot (Figure. S2, supplementary material). The molecular dynamics simulation analysis of the refined LIMK2-TH300 complex showed that the system has attained the least RMS deviations of $\sim$ 0.35 nm initially (Figure 2a). After $\sim$74 ns the system showed higher deviations of $\sim$ 0.6 nm, however, from $\sim$130 ns it has equilibrated well and tends to converge till the end of the MD production run. The RMS deviations of the LIMK2-TH300 complex tend to be highly converged and well equilibrated than *apo* LIMK2 (Figure S4a, supplementary material). In the case of protein-ligand RMSD analysis (Figure S3a, supplementary material), the well-equilibrated ligand has shown the least deviations of $\sim$ 0.18 nm with a higher degree of convergence, whereas the LIMK2 has shown higher deviations of $\sim$ 0.6 nm. Subsequently, on analyzing the domain-based backbone RMSD of LIMK2 (Figure 2b), it was observed that the C lobe domain features a higher RMS deviation of $\sim$ 0.6 nm, than the N lobe domain which is well equilibrated with the least RMS deviation of $\sim$ 0.3 nm. This reveals that the higher deviation of the complex is highly due to the N-lobe of LIMK2. From the RMSF plot (Figure 2c), it was observed that overall, the C-Lobe residues feature higher fluctuations than the N-lobe residues. In specific, the loop segment of the C-lobe that follows the XDFG motif, namely the residues, Met485- Thr489 ($\sim$ 0.937 – 1.426) has shown higher fluctuations than that of the *apo* LIMK2 (Figure S4b, supplementary material). The inter-hydrogen bond interaction

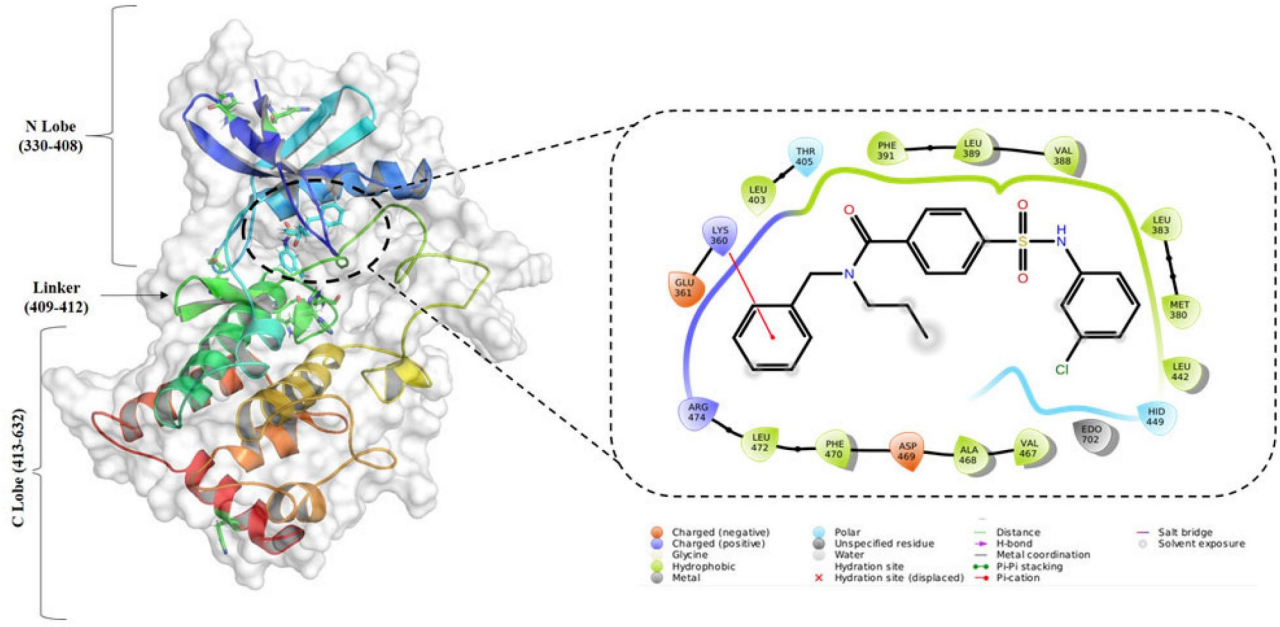

Figure 1. Remodelled and refined LIMK2-TH300 complex (PDB ID: 5NXD) and the schematic representation of two-dimensional interaction of LIMK2 with TH300.

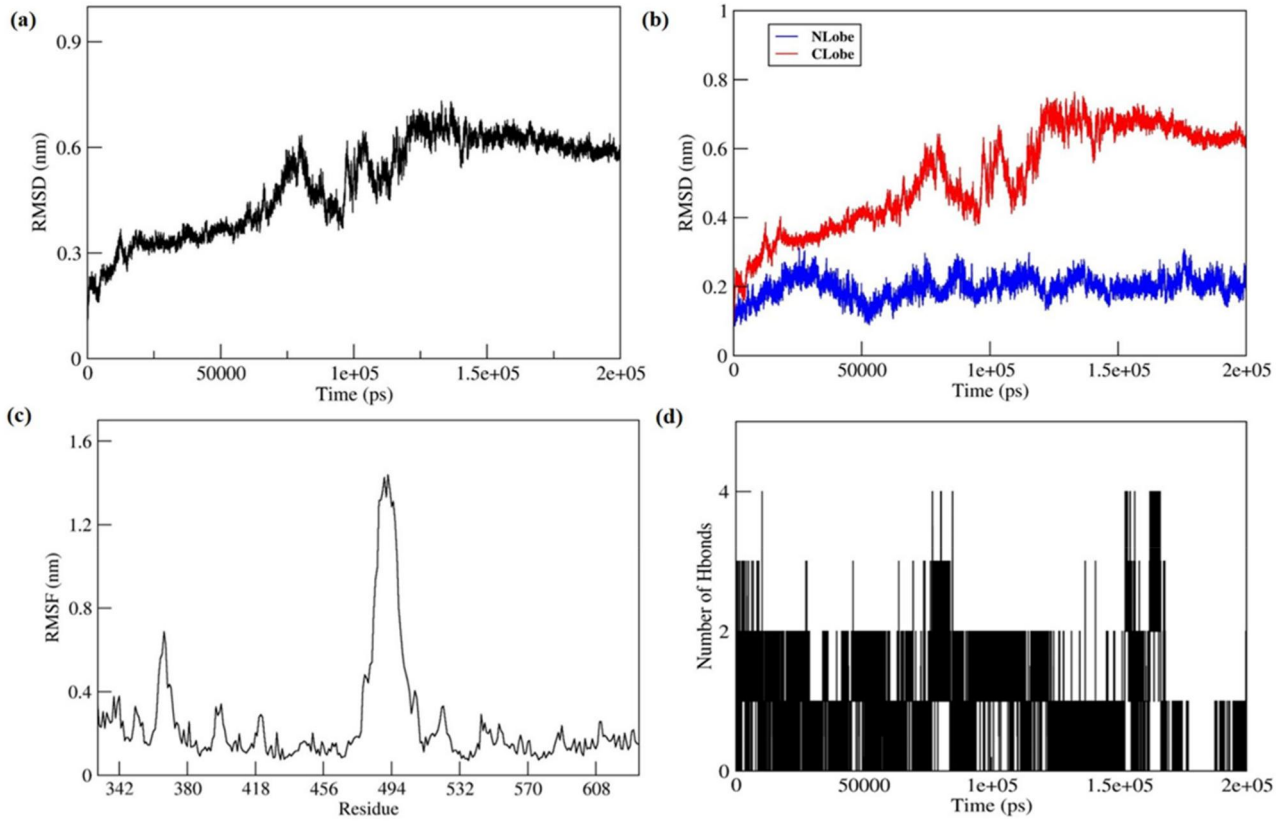

Figure 2. Molecular dynamics simulation analysis of LIMK2-TH300 complex (a) RMSD plot (b) Comparative RMSD analysis of Nlobe and Clobe of LIMK2 (c) RMSF analysis (d) inter-hydrogen analysis of LIMK2 with TH300.

analysis (Figure 2d**)** showed that nearly 4 H-bonds have attributed to the stability of the LIMK2- TH300 complex. However, on average only $\sim$ 2 H-bonds are maintained throughout the MD production run. The FEL analysis resulted in only one near-native cluster (Figure 3a), which represents the stable conformation of the complex. In the analysis of the FEL contour plots for both the *apo* (Figure S5a, supplementary material) and the allosteric inhibitor (TH300)-bound state of LIMK2 (Figure 3a), it was observed that, the *apo* LIMK2 exhibited two near-native clusters, whereas the TH300-bound state showed a single near-native cluster. This suggests that *apo* LIMK2 has a greater capacity for undergoing conformational transitions compared to the inhibitor-bound state. A structural comparative analysis of the near-native conformations of *apo* LIMK2, extracted at the

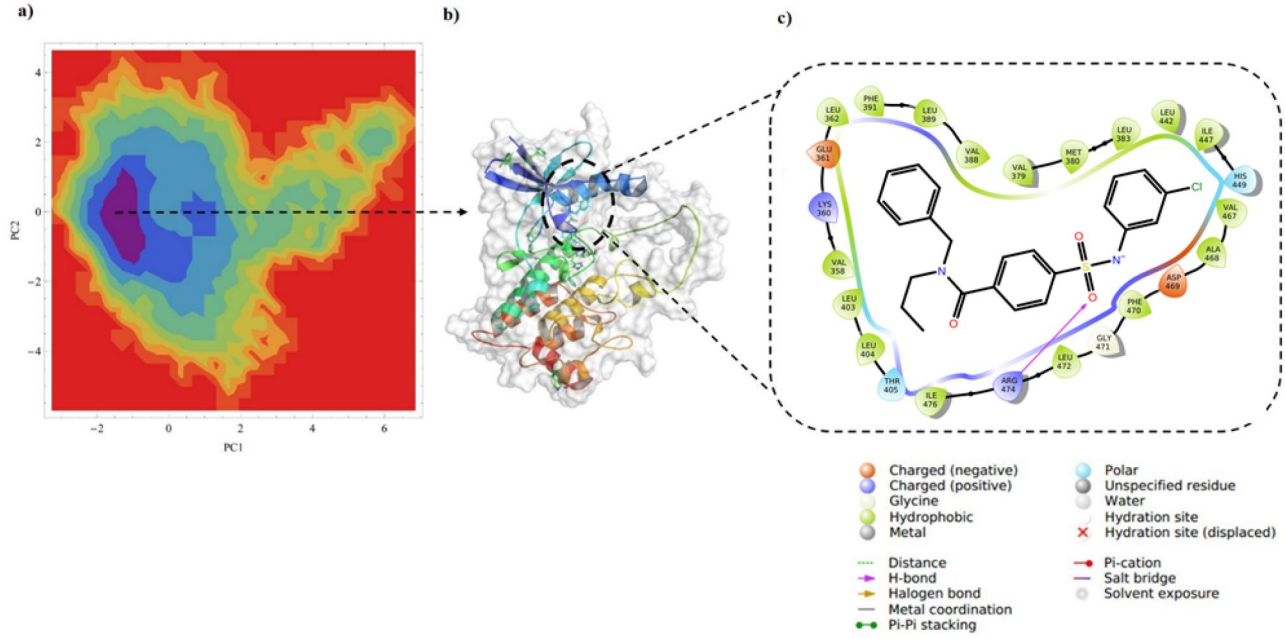

Figure 3. (a) 2D contour free energy Landscape plot of LIMK2-TH300 complex (b) Representative near-native conformation of LIMK2-TH300 complex obtained at 76th ns (c) 2D interaction analysis of near-native LIMK2-TH300 complex.

49.5th ns (near-native cluster 1) and 64th ns (near-native cluster 2), revealed that these conformational states were primarily influenced by transitions in the loop segment (A468-A514) composed of XDFG and the activation loop (a.l) (Figure S5b, supplementary material). In the case of LIMK2-TH300, only one near-native cluster was observed, indicating that the interactions of TH300 with the XDFG residues (A468-G471) and L472, as well as Arg474 (a.l), contributed to the restricted movement of the loop segment (A468-A514). Upon a comparative interaction analysis of the representative near-native conformation of the LIMK2-TH300 complex extracted at the 76th ns (Figure 3b), in comparison to the initial conformation, it was observed that only Arg474 (of a.l) maintained a stable hydrogen bond with TH300 (Figure 3c).

Pharmacophore-based virtual screening

In this study, an energetically optimized ligand-based pharmacophore hypothesis was generated for selected reference compound (TH300) from their corresponding retrieved frames to extract features of Type III inhibitor for LIMK2. The generated hypothesis had five featured pharmacophores (RRRAH), including three aromatic rings (R7, R8, R9), one hydrophobic group (H6), and one hydrogen bond acceptor (A3) as shown in Figure 4 with reference ligand for the best pharmacophore model.

After undergoing all primary filtration processes, the filtered compounds were then subjected to virtual screening with the generated pharmacophoric hypothesis. Among the compounds, only 8,35,500 compounds satisfy the four Pharmacophoric features as that of the reference ligand. Following the HTVS and SP Mode, the resulting compounds were further subjected to XP Mode, which resulted in 557 compounds (the top 10% of the SP mode). After the overall filtration process, based on the docking score, glide energy, and fitness score, among the top 10 compounds (Table 1**)**, except for compounds ZINC1349067047, ZINC1649903059, and ZINC735522383 with low fitness score, the other compounds were considered for ADME/Tox analysis. Amongst the 7 compounds (Tables 2 and 3), only five compounds exhibited better pharmacokinetic properties: ZINC1044382792, ZINC1433610865, ZINC1044109145, ZINC952869440), and ZINC490621334. Therefore, the five identified compounds (Table 4) were subjected to re-ranking based on their Molecular Mechanics Generalized Born Surface Area (MM/GBSA) score. It was observed that ZINC1433610865 and ZINC1044109145 have significant binding free energy scores of − 45.61 kcal/mol and −45.89 kcal/mol, respectively and also which has higher than the other compounds. In summary, the calculated binding free energy of the protein-ligand complexes is within the range of − 31.32 kcal/mol to − 45.89 kcal/mol. Based on the MM/GBSA analysis, it can be concluded that the van der Waals (ΔG_{VdW}) and coulomb (ΔG_{col}) terms are the primary contributors to the favorable binding of the ligands to the LIMK2 (Table S1, supplementary material). The binding mode analysis of the complexes **(**Table 4 & Table S2, Figure 5**),** infers that in LIMK2-ZINC1044382792 complex the amine group of the residue Asp469 shared a hydrogen bond (2.29 Ð) to the amine group of the ligand molecule. The other hydrogen bonds were formed by the carbonyl group of the residues Glu406 and Ile408 with the amine group of the ligand with a distance of 2.62 Ð and 1.77 Ð respectively. Moreover, the LIMK2-ZINC1044382792 complex stability was enhanced by the hydrophobic residues including Leu337, Val358, Met380, Leu389, Phe391, Leu403, Tyr407, Leu458, Val467, Ala468, Phe470, and Leu472. While binding mode analysis of the LIMK2-ZINC1433610865 complex revealed the four hydrogen bonds and it was found that the carbonyl group of the residue Asp469 formed the hydrogen bond with the amine group of the ligand (2.31 Ð). Another interaction was observed between the amine group

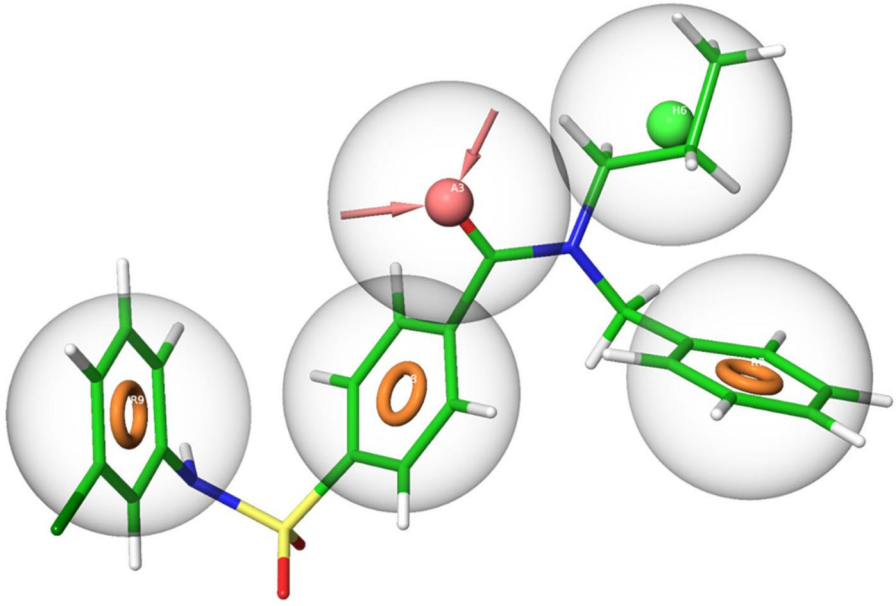

Figure 4. Pharmacophore hypothesis of the reference ligand (TH300).

Table 1. Summary of the top-ranked compounds based on their docking score, docking energy, and phase screen score obtained from virtual screening studies.

Compound ID	Num Sites Matched	Matched Ligand Sites	Align Score	Fitness	Phase Screen Score	XP GScore	Glide gscore	Glide Energy (kcal/mol)	glide emodel (kcal/mol)
ZINC1044382792	4	A(6) H(11) R(13) R(12) R(–)	1.19	1.28	1.28	−9.13	−9.13	−44.27	−62.03
ZINC1433610865	4	A(6) H(10) R(13) R(12) R(–)	0.8	1.63	1.63	−8.33	−8.33	−44.54	−62.86
ZINC1044109145	4	A(6) H(11) R(12) R(13) R(–)	1.04	1.18	1.18	−7.74	−7.74	−44.53	−63.75
ZINC952869440	4	A(3) H(8) R(9) R(10) R(–)	0.90	1.33	1.33	−7.70	−7.70	−38.33	−56.77
ZINC490621334	4	A(7) H(9) R(11) R(13) R(–)	1.34	1.06	1.06	−7.31	−7.31	−40.07	−59.33
ZINC1418471164	4	A(5) H(9) R(11) R(12) R(–)	0.95	1.11	1.11	−9.31	−9.31	−49.00	−66.39
ZINC1349067047	4	A(4) H(7) R(9) R(8) R(–)	1.13	0.69	0.69	−9.27	−9.27	−41.11	−59.43
ZINC1649903059	4	A(3) H(10) R(12) R(–) R(11)	1.52	0.72	0.729	−9.19	−9.19	−47.54	−69.17
ZINC735522383	4	A(4) H(10) R(11) R(–) R(12)	1.43	0.66	0.66	−9.07	−9.07	−47.21	−69.92
ZINC951446194	4	A(5) H(11) R(13) R(12) R(–)	0.64	1.22	1.22	−9.07	−9.07	−42.12	−55.20

Table 2. ADME analysis and pharmacological properties of screened top-ranked compounds.

[a]Compound ID	[b]Mol MW	[c]donorHB	[d]acceptHB	[e]QPlogS	[f]QPlogPw	[g]Qplog Po/w	[h]QPlogHERG	[i]QPPCaco	[j]Qplog BB	[k]QPP MDCK	[l]Percent of HOA
ZINC1044382792	289.296	2	8.2	−3.25	13.91	0.465	−5.08	111.98	−1.60	46.41	66.343
ZINC1433610865	294.313	3	9.4	−2.419	15.14	0.177	−4.73	119.79	−1.84	49.91	65.181
ZINC1044109145	295.318	2	9.2	−3.013	14.42	−0.117	−4.69	79.35	−1.65	55.95	60.262
ZINC952869440	292.297	1	8.5	−2.352	11.77	0.513	−3.96	315.54	−0.99	142.19	74.678
ZINC490621334	273.257	1	9	−2.468	12.73	−0.242	−4.73	97.99	−1.67	40.17	61.166
ZINC1418471164	292.3	2	10.5	−0.812	14.96	−1.186	−5.09	16.019	−1.567	6.276	41.563
ZINC951446194	290.284	2	8	−2.802	12.942	−0.185	−4.384	22.678	−2.386	8.259	50.123

[a]Compound ID.
[b]Molecular weight, in Da (range for 95% of drugs: 130–725 Da).
[c]No: of Hydrogen bonds donated by the molecule (range for 95% of drugs: 0–6).
[d]No: of Hydrogen bonds accepted by the molecule (range for 95% of drugs: 2–20).
[e]Predicted aqueous solubility; S in mol/L (acceptable range: −6.5 to 0.5).
[f]Predicted water/gas partition coefficient (acceptable range: 4.0 to 45.0).
[g]Predicted octanol/water partition co-efficient log P (acceptable range: −2.0 to 6.5).
[h]log HERG, HERG K + channel blockage (concern below −5).
[i]Apparent Caco-2 permeability (nm/s) (<25 poor, >500 great).
[j]Predicted brain/blood partition coefficient (acceptable range: −3.0 to 1.2).
[k]Apparent MDCK permeability (nm/s) (25 poor, >500 great).
[l]Percentage of human oral absorption (<25% poor and >80% is high).

of the residue Phe391 and the carbonyl group of the ligand with a distance of 1.86 Ð. Meanwhile, there are two hydrogen bonds were noted in the residue Leu389 from the carbonyl group to the hydroxyl group of the ligand. The additional hydrophobic residues (Ala345, Val358, Met359, Leu362, Met380, Leu383, Val388, Leu403, Phe470, Leu472, and Arg474) are present in the binding pocket to aid the stable binding of the complex. In the LIMK2-ZINC1044109145 complex, it was observed that the amine group of the ZINC1044109145 moiety formed a hydrogen bond with the carbonyl group of Asp469 at a distance of 2.31 Ð. Also, the same residue was found with another hydrogen bond interaction from the amine group to the ligand's hydroxyl group with a distance of 2.36 Ð. Also, it could be noted that the residue Lys360 formed the

Table 3. Swiss ADME/Tox analysis and pharmacological properties of Screened top ranked compounds.

S. No	Compound Code	MW (g/mol)	HBd	HBa	LogP	LogS	GI Absorption	Leadlikliness	TPSA (Å^2)
1.	ZINC1044382792	289.29	3	6	0.74	−1.29	High	Yes	119.92
2.	ZINC1433610865	294.31	3	6	1.23	−0.03	High	Yes	118.09
3.	ZINC1044109145	295.32	3	3	0.83	−1.90	High	Yes	148.16
4.	ZINC952869440	292.29	1	5	1.99	−1.08	High	Yes	103.81
5.	ZINC490621334	273.25	1	7	1.60	1.60	High	Yes	116.30
6.	ZINC1418471164	292.30	2	7	1.72	−0.66	Low	Yes	121.69
7.	ZINC951446194	290.28	3	6	0.21	−0.99	Low	Yes	132.55

Table 4. The optimal binding free energy score and interaction pattern analysis of the top obtained from virtual screening studies.

S.No.	Compound ID	MM/GBSA △G Bind (kcal/mol)	Hbond Interactions	Hydrophobic Residues	Other Non-Bonded Contacts
1	ZINC1044382792	−44.67	Glu406, Ile408, Asp469	Leu337, Val358, Lys360, Met380, Leu389, Phe391, Leu403, Thr405, Tyr407, Gly411, Leu458, Val467, Ala468, Phe470, Leu472	Lys360, Thr405, Gly411
2	ZINC1433610865	−45.61	Leu389, Phe391, Asp469	Ala345, Val358, Met359, Lys360, Leu362, Met380, Leu383, Val388, Lys390, Leu403, Thr405, Phe470, Gly471, Leu472, Arg474	Lys360, Lys390, Thr405, Gly471, Arg474
3	ZINC1044109145	−45.89	Asp469	Phe341, Met380, Leu383, Val388, Leu389, Lys390, Phe391, Leu403, Thr405, Leu442, Hsd449, Val467, Ala468, Phe470, Leu472	Lys360 (-cation), Lys390, Thr405, Hsd449
4	ZINC952869440	−31.32	Asp469, Arg474	Val358, Lys360, Glu361, Leu362, Met380, Leu383, Val388, Leu389, Phe391, Leu403, Thr405, Leu442, Val467, Ala468, Phe470, Gly471, Leu472	Lys360, Glu361, Thr405, Gly471
5	ZINC490621334	−44.90	Thr405, Asp469	Leu337, Phe342, Gly343, Val358, Lys360, Met380, Val388, Leu389, Phe391, Leu403, Thr412, Hsd455, Leu458,,Val467, Ala468, Phe470, Leu472	Gly343, Lys360, Thr412, Hsd455

π-cation interaction with the pyridine ring of the ligand molecule. Furthermore, the binding stability could be significantly improved by the presence of common hydrophobic residues, with Phe341, Met380, Leu383, Val388, Leu389, Phe391, Leu403, Leu442, Val467, Ala468, Phe470, Leu472 playing a crucial role in enhancing complex stability. The LIMK2-ZINC952869440 complex showed the hydrogen bond was noticed between the amine group of the ligand and the carbonyl group of residue Asp469, at a distance of 1.94 Ð. In the meantime, the complex exhibited an interaction, where the amine group of the Asp469 formed a hydrogen bond with the carbonyl group of ligand (1.85 Ð). Additionally, the amine group of the residue Arg474 interacted with the carbonyl group of the ligand by hydrogen bond formation. As well, the complex stability was also enhanced by the hydrophobic residues Val358, Leu362, Met380, Leu383, Val388, Leu389, Phe391, Leu403, Leu442, Val467, Ala468, Phe470, and Leu472. The LIMK2- ZINC490621334 complex revealed the interaction pattern of three hydrogen bonds. Among the three interactions, the residue Asp469 exhibited the two interactions, and the first interaction was observed between the amine group of the ligand and carbonyl group of the residue distance with 2.41 Ð. The second interaction was found from the nitrogen atom of the ligand to the amine group of the Asp469 (2.00 Ð). The additional interaction was to be noticed with the distance of 1.92 Ð from the hydroxyl group of the ligand to the hydroxyl group of the residue Thr405. Furthermore, it is worth mentioning that the complex's binding stability is ensured by the presence of hydrophobic residues, such as Leu337, Phe342, Val358, Met380, Val388, Leu389, Phe391, Leu403, Leu458, Val467, Ala468, Phe470, and Leu472. These residues play a crucial role in enhancing the stability of the complex. The results indicate that the identified inhibitors exhibits a higher binding affinity to the protein and forms stable hydrogen bonds with the protein. Importantly, all of these hydrogen bonds were found to be formed within a proximity of 3 Ð, suggesting favorable interaction between the inhibitors and the protein.

Overall, the interaction analysis of the identified compounds (Table 4 & Table S2, Figure 5), showed that Asp469 ('D' FG motif), Leu389 (b.I), Phe391 (β4), Thr405 (G.K), and hinge residues, namely, Glu406, Ile408 of LIMK2 were observed to have formed hydrogen bonds with the compounds. Other than hydrogen bonds, only the compound ZINC1044109145 has been observed to have crucial π-cation interaction with Lys360 (βIII). Further, for the prioritized top five identified compounds, each of these in complex with LIMK2 was subjected to molecular dynamics (MD) simulation analysis to assess the stability of the complex formation.

Density functional theory

Density Functional Theory calculations of the identified top compounds were performed to determine the chemical reactivity and stability based on their theoretical energies of frontier molecular orbitals. Table 5 depicts the identified top compounds' molecular orbitals, including HOMO, LUMO, and Gap energy. Further, the stereo electronic properties and atomic contribution of the top compounds were examined, and respective plots were shown in Figure S6 & Figure 6. The calculated theoretical energies indicate that the gap energy for all the compounds obtained is within an average range of − 0.08 eV to − 0.23 eV, which implies their molecular reactivity. Among the shortlisted compounds, compound

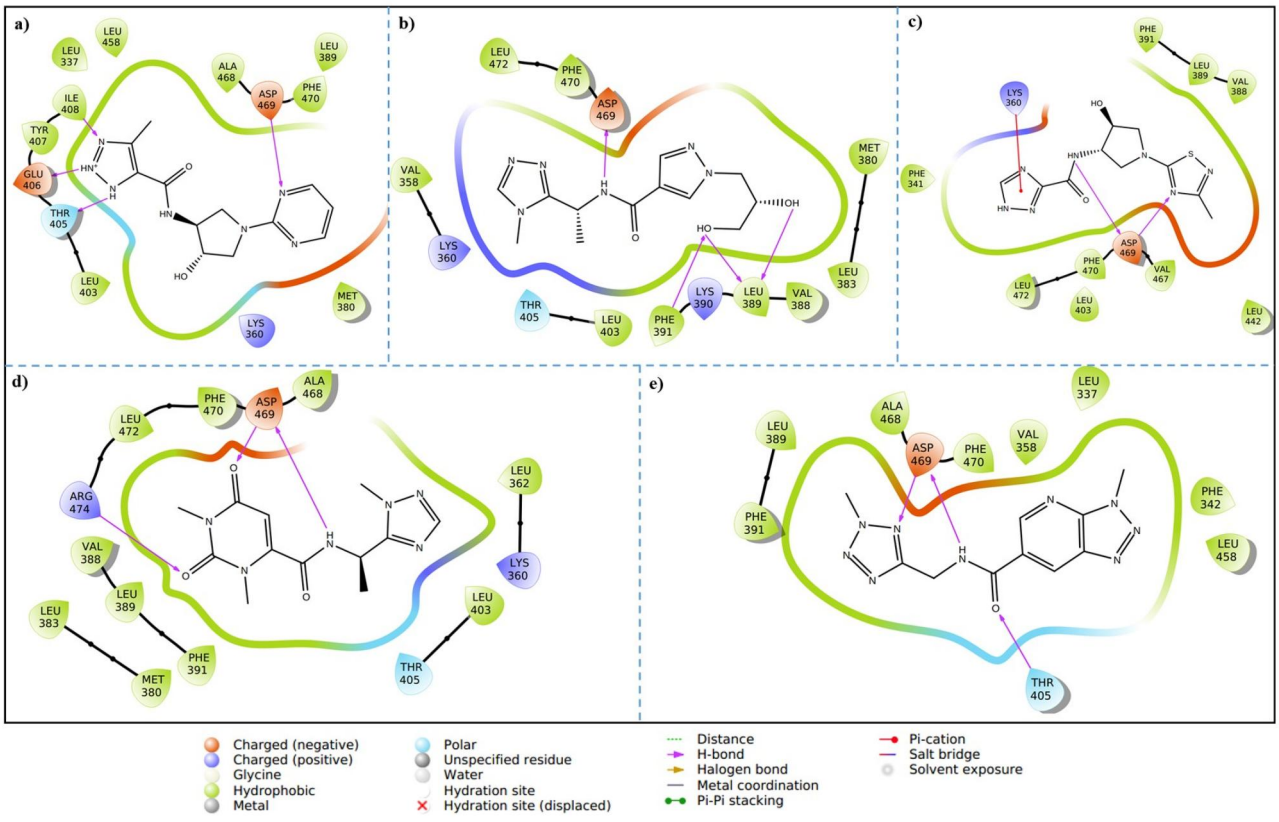

Figure 5. Schematic 2D interactions of the LIMK2 protein with the top ranked ZINC database compounds (a) compound ZINC1044382792, (b) compound ZINC1433610865, (c) compound ZINC1044109145, (d) compound ZINC952869440, (e) compound ZINC490621334.

Table 5. Density Functional Theory Analysis of top ranked compounds with the occupancy of HOMO and LUMO profiles and gap (HLG eV).

S. No.	Compound ID	HOMO (eV)	LUMO (eV)	HLG (eV)
1.	TH300	−0.2567	−0.1744	−0.0823
2.	ZINC1044382792	−0.2174	−0.0439	−0.1735
3.	ZINC1433610865	−0.2545	−0.0234	−0.2311
4.	ZINC1044109145	−0.2256	−0.0415	−0.1841
5.	ZINC952869440	−0.2476	−0.0708	−0.1768
6.	ZINC490621334	−0.2607	−0.0822	−0.1785

2 (ZINC1433610865) was observed with the least HOMO-LUMO energy gap value was found to be

– 0.23 eV has exhibited higher electron accepting ability (LUMO energy) and lower electron-donating capability (HOMO energy). Moreover, it was observed that the HOMO energy of the top five compounds is greater than their LUMO energy and the reference inhibitor also scored lower gap energy than the identified compounds. These results indicate a substantial donor quality of the compounds that results in a robust and stable interaction between the compounds and the LIMK2 protein.

Molecular dynamics simulation analysis of the complexes

On comparative analysis of the LIMK2-inhibitor complexes, it was observed from the RMSD plot (Figure 7a), that the LIMK2-ZINC952869440 complex showed higher RMS deviations of ∼ 0.62 nm followed by LIMK2-ZINC1044109145 complex with the deviation of ∼ 0.58 nm than other complexes. However, complexes LIMK2-ZINC952869440 and LIMK2-ZINC1044109145 have attained equilibrium after ∼ 50 ns and ∼ 86 ns, respectively, and have tended to converge till the end of the MD production run. In contrast, the other complexes are observed to be well equilibrated with a least RMS deviation of ∼ 0.45 nm. On analyzing the LIMK2 and inhibitor RMSD profiles (Figure S3b-f, supplementary material), all the inhibitors were observed to be well equilibrated and converged with the least RMS deviations than LIMK2. In the case of LIMK2 domain-based RMSD profiling (Figure S7a & S7b, supplementary material), the N-lobe of LIMK2-ZINC1044109145 complex has shown higher RMS deviations of ∼ 0.56 nm, while the C-lobe of LIMK2-ZINC952869440 complex showed higher RMS deviations of ∼ 0.60 nm than other complexes. This elucidates that the respective RMS deviations of these complexes have been highly attributed to the drastic RMS deviation of the C-Lobe. From the comparative RMSF plot analysis (Figure 7b, Figure S7c & S7d, supplementary material), it was inferred that the C-lobe residues have exhibited higher fluctuation than the N-lobe, in specific, the loop segment of the C-lobe, namely, Met485-Thr489 (∼ 0.76 – 1.24 nm) has shown higher fluctuations. However, amongst the complexes, the higher fluctuations were observed in LIMK2-ZINC952869440 (∼ 1.24 nm), while minimal fluctuations were observed in complexes LIMK2-ZINC1044382792 and LIMK2- ZINC490621334. In the distance analysis of the inhibitor(s) with LIMK2 (Figure 7c**),** it was inferred that except for inhibitor ZINC952869440 with a higher deviation of ∼ 0.6 nm at ∼100-150 ns, the other inhibitors were found to maintain stable distance with the LIMK2 (∼0.1-0.4 nm), which infers that the LIMK2-ZINC952869440

Table 6. Contact map analysis of the inhibitors with LIMK2.

	Residue No	Residue Name	TH300	ZINC 1044382792	ZINC 1433610865	ZINC 1044108145	ZINC 952869440	ZINC 490621334
β1	337	LEU	2.6	100	0.6	8.6	99.7	99
g.l	339	LYS	0	0	0	0	4.7	0
	340	GLY	0	0	0	0	5.7	0
	341	PHE	2.9	54.5	0	9.3	39.4	10.4
	342	PHE	98.8	99.6	0.1	8.7	93	74
	343	GLY	0.1	93.1	0	0.3	30.3	46.4
β2	344	GLN	0.5	82.3	5	0.6	28.2	18.2
	345	ALA	99.8	100	95.5	3.8	98.9	99.2
	346	ILE	92.8	33	4.4	0	11.8	1.4
β3	357	MET	0	1.7	0	0	12.5	0
	358	VAL	99.9	100	98.2	9	100	100
	359	MET	97.8	99.5	95.2	0.2	98.1	71.7
	360	LYS	100	100	99.9	97.1	100	100
	361	GLU	99.8	0.1	0	83.5	1.2	46.3
	362	LEU	100	0	65.2	73.8	9.9	41
αC	373	PHE	1	0.7	6.7	37.3	4.9	3.1
	376	GLU	2	0	0.5	0	1.8	0.1
	377	VAL	0	0	3.3	2.6	1	0
	379	VAL	98	0	23	0	0	20.3
	380	MET	100	2.5	100	95.7	5	99.7
	381	ARG	0.1	0	38.9	0	0	9.3
b.l	383	LEU	100	0.7	100	96	0	55.1
	387	ASN	0.2	0	4.1	4.1	0	0
	388	VAL	100	1.1	100	100	0	52.7
	389	LEU	100	100	100	100	97.3	99.4
	390	LYS	3.4	1.2	93.6	96.8	2.9	26.7
β4	391	PHE	100	94.4	100	100	82.8	99.8
	392	ILE	0.5	14.9	23	14.2	1.4	0.4
	393	GLY	0	6.8	9.4	0.3	0.8	0
	394	VAL	0	0.1	0.2	1.2	0.1	0
β5	402	ASN	96.6	0.5	0	0.2	1.2	11.9
	403	LEU	100	99.7	100	100	98.7	100
	404	LEU	97.5	95.4	98.8	56.1	88.3	46.9
GK	405	THR	100	100	100	100	100	100
Hinge	406	GLU	0.3	100	0.6	23.3	96.3	8.4
	407	TYR	0.1	100	0	5.9	98.7	30.9
	408	ILE	0.1	100	0	6.9	99.8	29.4
αE	441	TYR	0	0	6.8	0.1	0	4.6
	442	LEU	100	0.2	100	100	0	43.9
β6	447	ILE	100	0	99.6	57.2	0	29.3
	448	ILE	96.4	0	0	0.9	0	0.6
c.l	449	HSD	100	0	80.8	96.2	0	11.1
	450	ARG	0.2	0	0	0	0	0
	451	ASP	0.5	0	0	0	0	0
	452	LEU	0.2	0	0	9.2	0	0
	456	ASN	0.2	6.5	0	5.1	3	14.6
β7	458	LEU	1.2	100	0	15.6	98.2	75.9
β8	467	VAL	100	1.9	71.7	99.9	0.8	21
X	468	ALA	100	39.4	94.4	100	65.9	62.1
D	469	ASP	100	99.9	100	100	86.6	99.9
F	470	PHE	100	100	100	100	100	100
G	471	GLY	100	68.2	99.9	53.2	54.8	45.3
a.l	472	LEU	100	98.1	100	99.4	99.9	100
	473	SER	1.9	0	96.5	0.8	0.1	3.7
	474	ARG	100	48.5	100	82.2	38.9	52.3

complex might have lost the crucial interactions that aid in the stability of the complex. From the comparative inter-hydrogen bond analysis of the LIMK2-inhibitor complexes (Figure 7d), it was observed that amongst the complexes only LIMK2-ZINC1433610865 had maintained nearly ∼ 5 H-bonds, followed by LIMK2- ZINC1044382792 complex with ∼ 4 H-bonds throughout the MD production run, while other complexes have maintained only ∼ 2-3 H-bonds to stabilize the complexes.

Essential dynamics analysis

The interaction analysis of LIMK2-ZINC1044382792 complex near-native conformation extracted at 124.28th ns (Figure 8), reveals the residues Phe342, Glu406, and Ile408 to form interactions through hydrogen bonds, significantly contributing to the overall stability of the complex. Moreover, a strong affinity for complex formation was observed due to the presence of hydrophobic residues, specifically Leu337, Phe342, Ala345, Val358, Met359, Leu389, Phe391, Leu403, Leu404, Tyr407, Leu458, Phe470, and Leu472. Whereas the LIMK2-ZINC1433610865 complex extracted at 89.93rd ns, as depicted in Figure 9, displayed a high population and a strong hydrogen bond was observed to form with the residues Leu389, Val467, Asp469, and Arg474. Furthermore, an additional observation was made regarding this complex, where certain hydrophobic residues played a significant role in increasing complex stability. Specifically, the residues

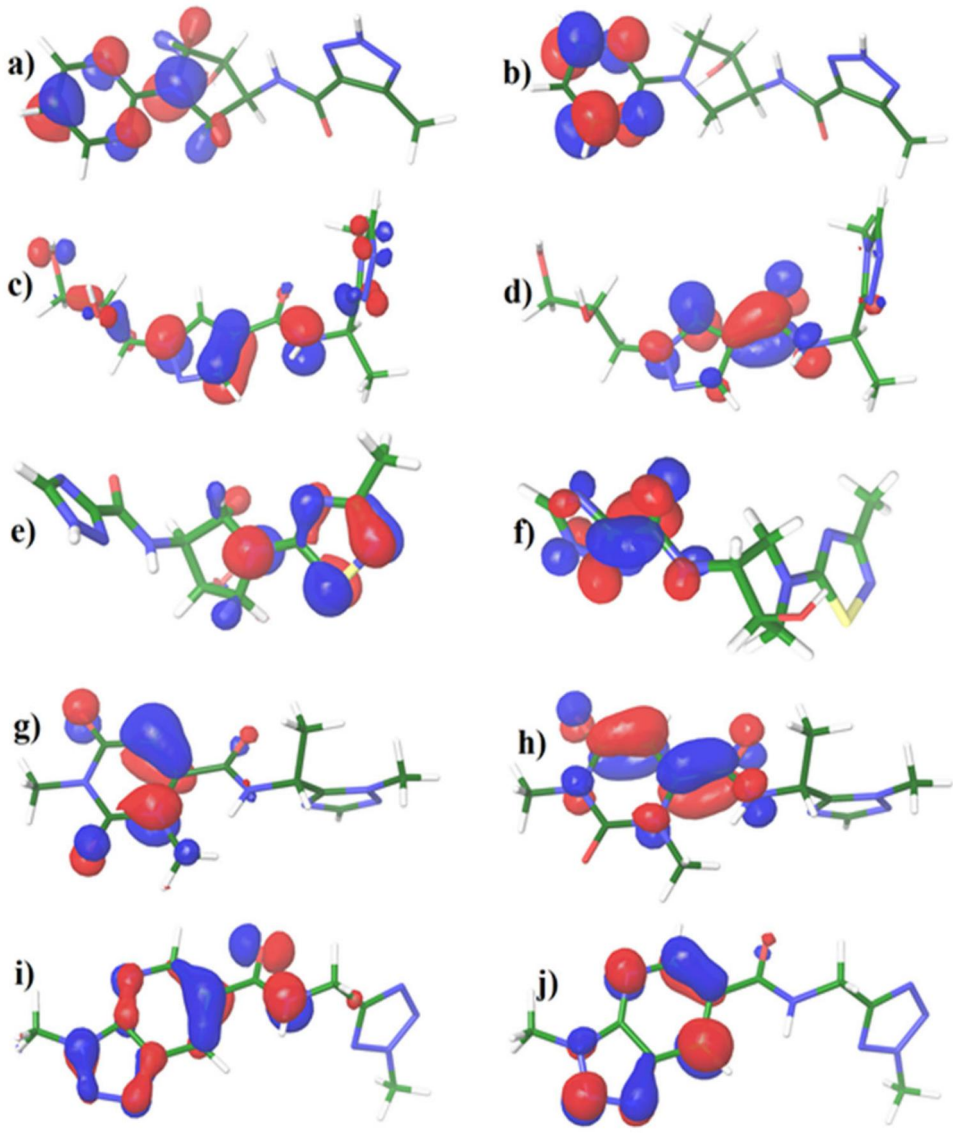

Figure 6. Density Functional Theory Analysis of top five compounds in complex with LIMK2 and its respective HOMO and LUMO profiles (a) HOMO and (b) LUMO of ZINC1044382792, (c) HOMO and (d) LUMO of ZINC1433610865, (e) HOMO and (f) LUMO of ZINC1044109145, (g) HOMO and (h) LUMO of ZINC952869440, (i) HOMO and (j) LUMO of ZINC490621334. The color representation in both orbitals, the blue color indicates positive and the red color indicates negative electron density of the compounds.

Ala345, Val358, Met359, Met380, Leu383, Val388, Leu389, Phe391, Leu442, Ile447, Ala468, Phe470, and Leu472 were found to contribute significantly to the overall stability of the complex. Similarly, the near-native conformation of the LIMK2-ZINC1044109145 complex (Figure 10) was obtained at 103.52nd ns. It revealed the crucial hydrogen bond formation from the ligand to the residue Asp469 to aid the maintenance of structural stability. Moreover, the hydrophobic residues: Phe341, Ala368, Met380, Leu383, Val388, Leu389, Phe391, Leu403, Thr405, Val467, Phe470, and Leu472 had significant interactions with the ligand to enhance the stability of the complex. The LIMK2-ZINC952869440 complex, extracted at 72nd ns represented in Figure 11, exhibited a near-native conformation. In this conformation, a hydrogen bond was observed to form with the active site residue Ile408. Additionally, it was noted that the hydrophobic residues Leu337, Phe342, Ala345, Val358, Leu389, Leu403, Tyr407, Leu458, Ala468, Phe470, and Leu472 played a crucial role in enhancing the structural affinity of the complex with the compound. However, the LIMK2-ZINC490621334 complex (Figure 12) exhibited the near-native conformation at 98.65th ns with no major hydrogen bonded interactions. Also, it was observed that residues such as Leu337, Ala345, Val358, Met380, Leu383, Val388, Leu389, Phe391, Leu442, Leu403, Ile447, Ala468, Asp469, Phe470, Leu472, Arg474 were involved in hydrophobic interactions, while π- π stacking and π- cation interactions formed by Phe470 and Arg474 were enhancing the stability and binding affinity of the complex.

Comparative analysis of the LIMK2-inhibitor complexes with reference inhibitor

The comparative RMSD profiling of LIMK2-inhibitor complexes (Figure S8a, supplementary material) inferred that all complexes have the least RMS deviations than the LIMK2-TH300 complex, which had a higher RMS deviation of ~

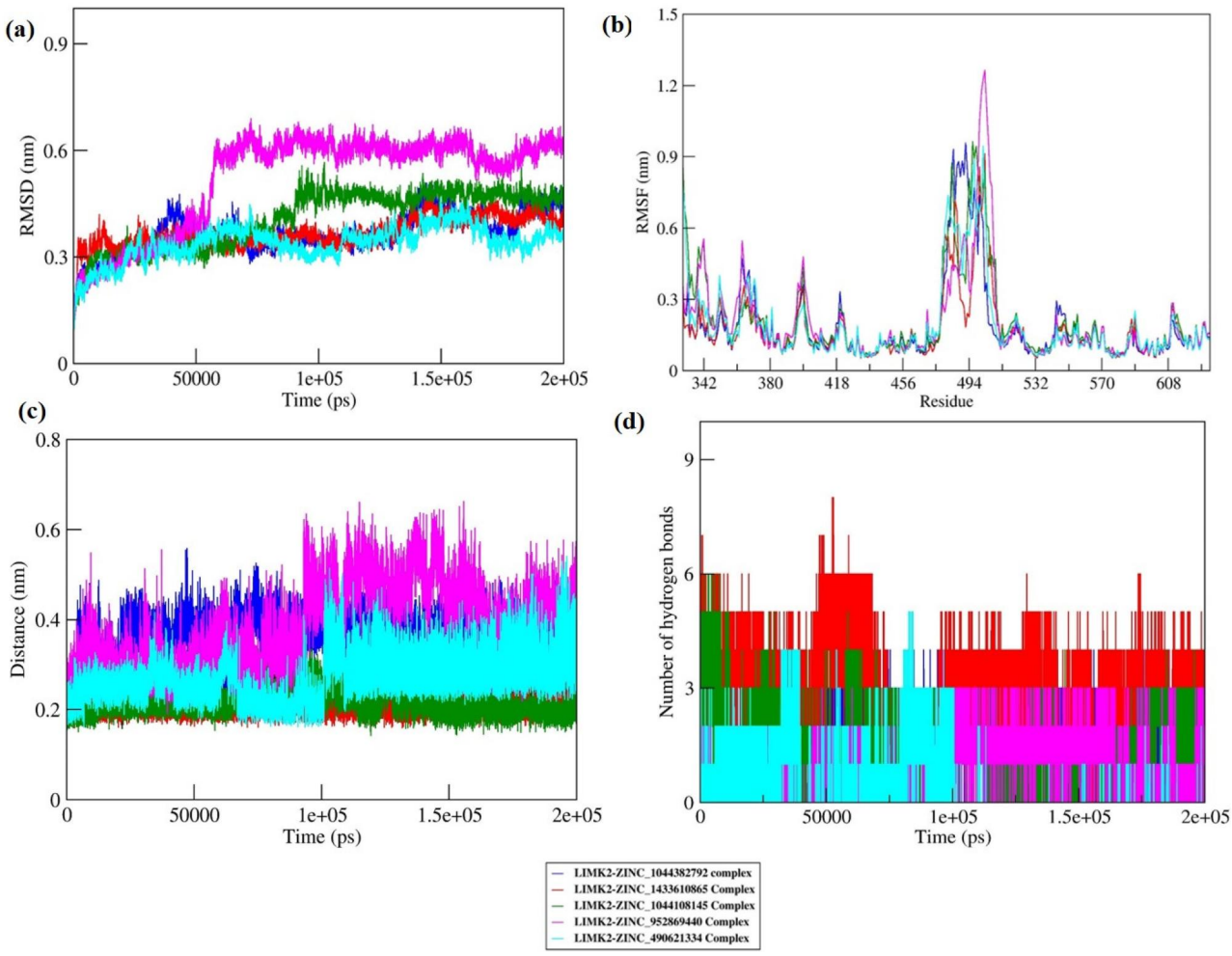

Figure 7. Molecular dynamics simulation analysis of LIMK2-inhibitor complexes (a) Comparative RMSD plot (b) Comparative RMSF analysis (c) Comparative distance analysis of the ligand with LIMK2 active site (d) Comparative inter-hydrogen analysis.

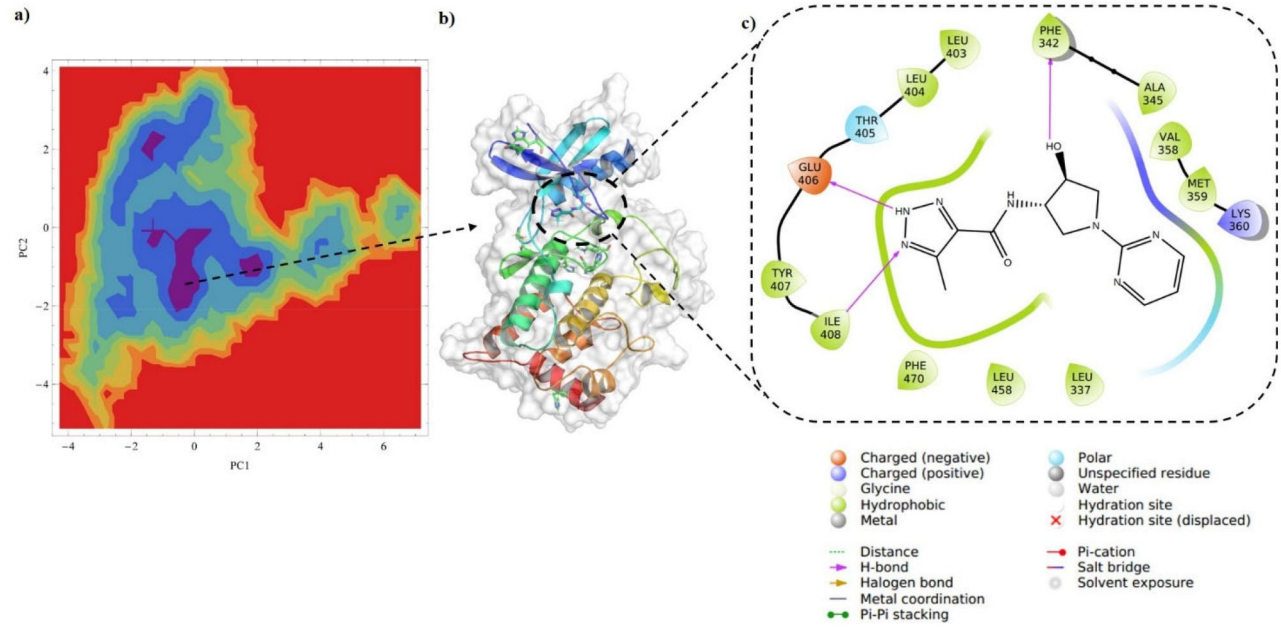

Figure 8. (a) 2D contour free energy Landscape plot of LIMK2-ZINC1044382792 complex (b) Representative near-native conformation of LIMK2- ZINC1044382792 complex obtained at 124.28th ns (c) 2D interaction analysis of near-native LIMK2- ZINC1044382792 complex.

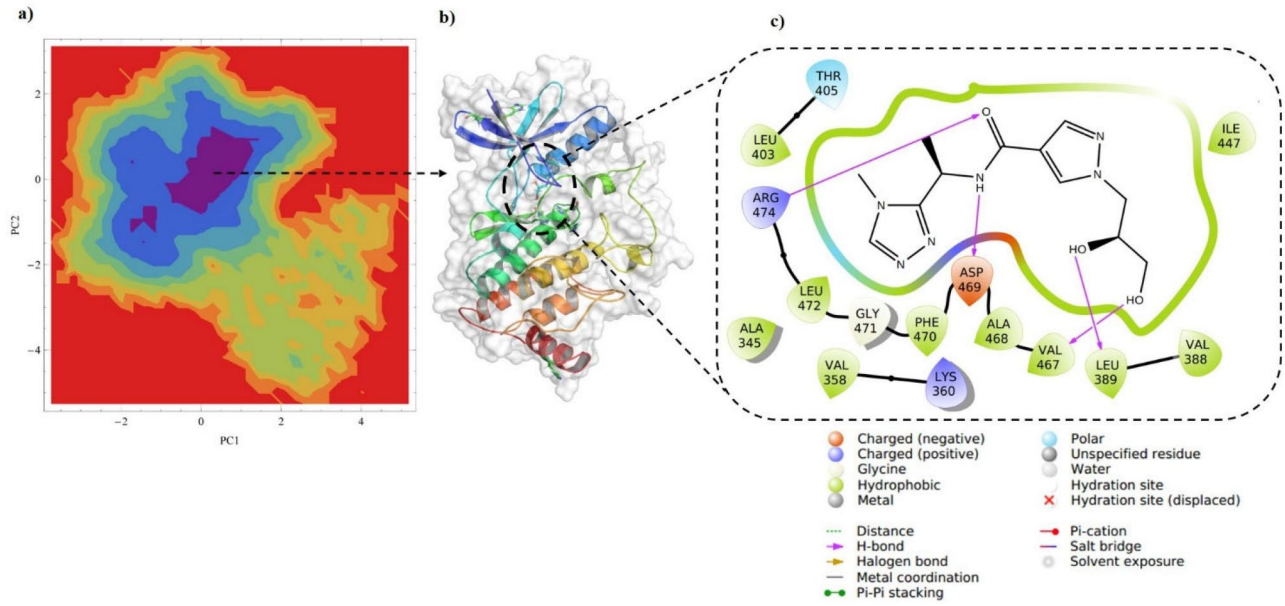

Figure 9. (a) 2D contour free energy Landscape plot of LIMK2-ZINC1433610865 complex (b) Representative near-native conformation of LIMK2- ZINC1433610865 complex obtained at 89.93rd ns (c) 2D interaction analysis of near-native LIMK2- ZINC1433610865 complex.

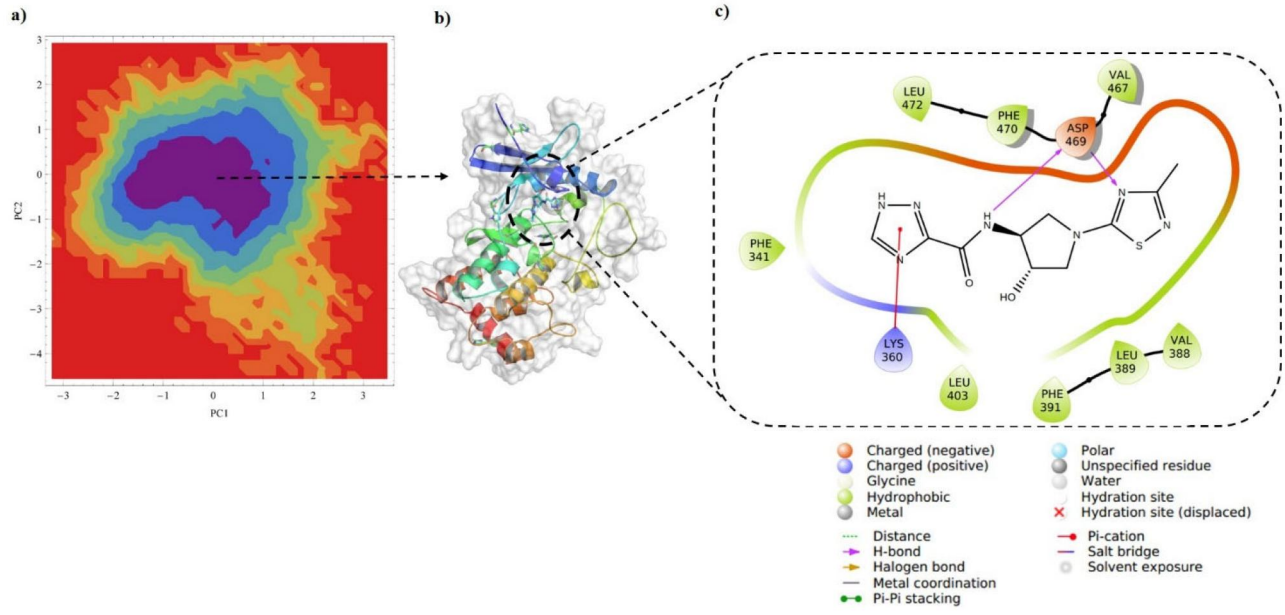

Figure 10. (a) 2D contour free energy Landscape plot of LIMK2-ZINC1044109145 complex (b) Representative near-native conformation of LIMK2- ZINC1044109145 complex obtained at 103.52nd ns (c) 2D interaction analysis of near-native LIMK2- ZINC1044109145 complex.

0.62 nm. Except for the LIMK2-ZINC952869440 and LIMK2-TH300 complexes, all the other complexes showed higher stability with the least RMS deviation. Moreover, the inter-hydrogen analysis (Figure S8b, supplementary material) also showed that amongst the complexes, only LIMK2-ZINC1433610865 and LIMK2-ZINC1044382792 complex were found to have maintained ∼ 5 H-bonds and ∼ 4 H-bonds throughout the MD production run than other complexes which maintained only ∼ 3 H-bonds as that of LIMK2-TH300 complex. On analyzing the H-bond occupancy of the interacting residues with ligands (Figure 13), it was observed that the residues Asp469 and Arg474, which highly aid in the stable interaction of TH300 with LIMK2, have maintained only 1% and 9.68% interactions throughout the MD production run. However, in other complexes, except for LIMK2-ZINC952869440 complex, the Asp 469 H-bond occupancy was observed in all complexes, in specific the higher occupancy of 12% was maintained by LIMK2-ZINC1433610865 complex. In the case of Arg474 H-bond formation, only LIMK2-ZINC1433610865 and LIMK2-ZINC490621334 showed H-bond occupancy as 28% and 1%, respectively. Apart from these residues, the complexes have also been observed to have crucial H-bond (Main-side chain) interactions with conserved kinase domain residues, in specific the compound ZINC1044382792 has maintained H-bond occupancy of nearly 29.27% and 41.73% with the Glu406 (hinge) and Phe342 (Glycine rich loop) respectively. At the same time, compound ZINC1433610865 has maintained a prominent H-

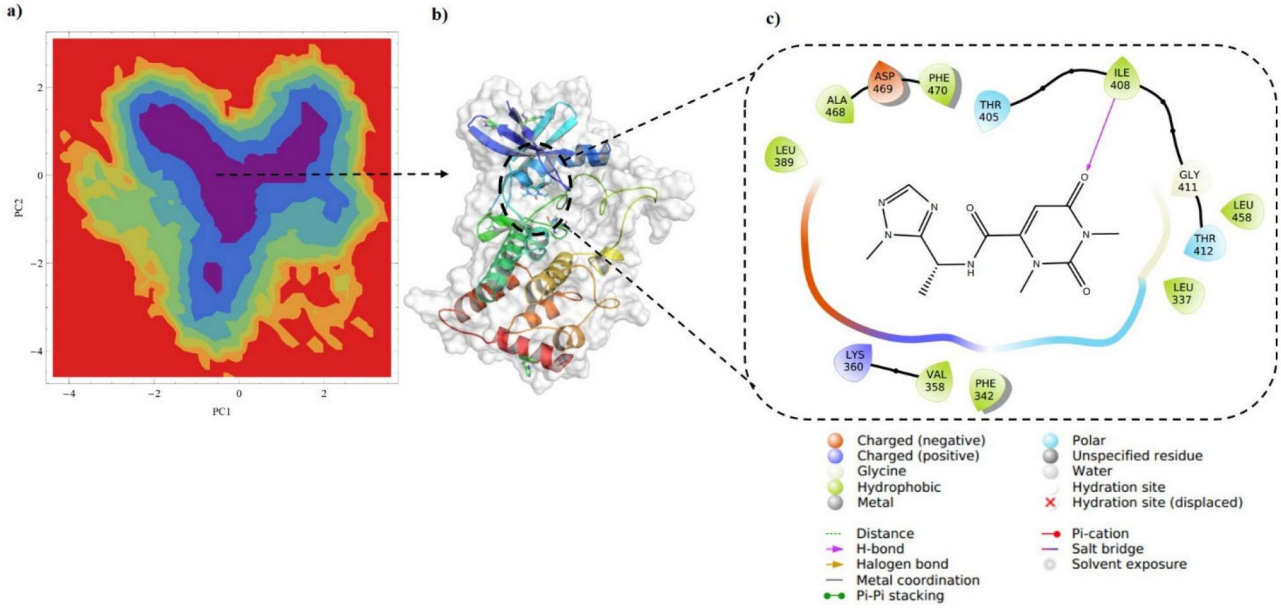

Figure 11. (a) 2D contour free energy Landscape plot of LIMK2-ZINC952869440 complex (b) Representative near-native conformation of LIMK2- ZINC952869440 complex obtained at 72nd ns (c) 2D interaction analysis of near-native LIMK2- ZINC952869440 complex.

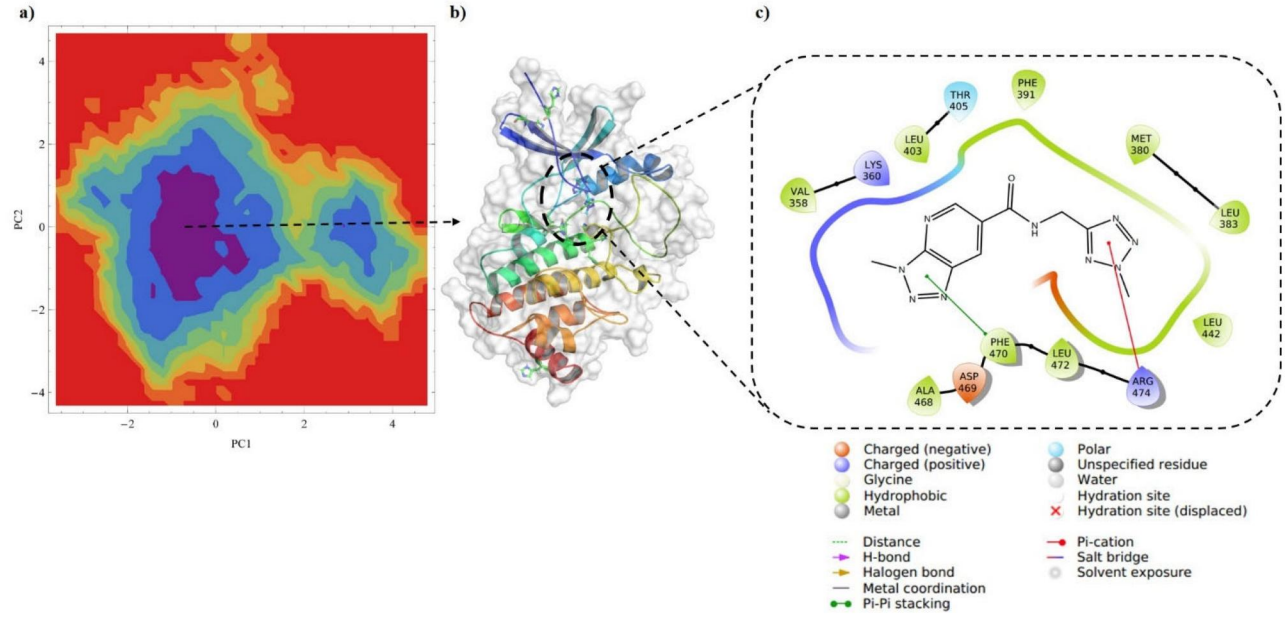

Figure 12. (a) 2D contour free energy Landscape plot of LIMK2- ZINC490621334 complex (b) Representative near-native conformation of LIMK2-ZINC490621334 complex obtained at 98.65th ns (c) 2D interaction analysis of near-native LIMK2-ZINC490621334 complex.

bond with Leu389 (b.l) and Met380 (αC) with an occupancy of 35.55% and 6.33% respectively. Other than this, compounds ZINC952869440 and ZINC1044108145 have maintained H-bond with hinge residue Ile408 (23.77%) and β3 residue Glu361 (5.30%), respectively.

Apart from the H-bonds, the other non-bonded contacts formed by the inhibitors with LIMK2 (within cut-off of 6 Å) were analyzed, (Table 6) and it was observed that the crucial residues Asp469 and Arg474 of LIMK2 to have maintained 100% contact with TH300 complex. In comparison with the TH300, except for ZINC952869440, with 86.6% contact with Asp469 ('D'FG motif), the other compounds showed 99.9% to 100% contact. On the other hand, Arg474 interactions were maintained at 100% in ZINC1433610865 as that of reference inhibitor TH300, while other compounds showed decreased contacts, specifically compound ZINC952869440, with the least contact of 38.9%. Except for ZINC1433610865 and ZINC1044108145, the glycine-rich loop (g.l loop) residues Phe342 were maintained in all other compounds. In the case of conserved β-sheet residues, the β5 residues that aid in hydrophobic interactions with the inhibitors have maintained greater contact in all compounds. However, the compound ZINC1044108145 has not maintained stable contact with β2, β3, and β6 residues as that of other inhibitors. The conserved

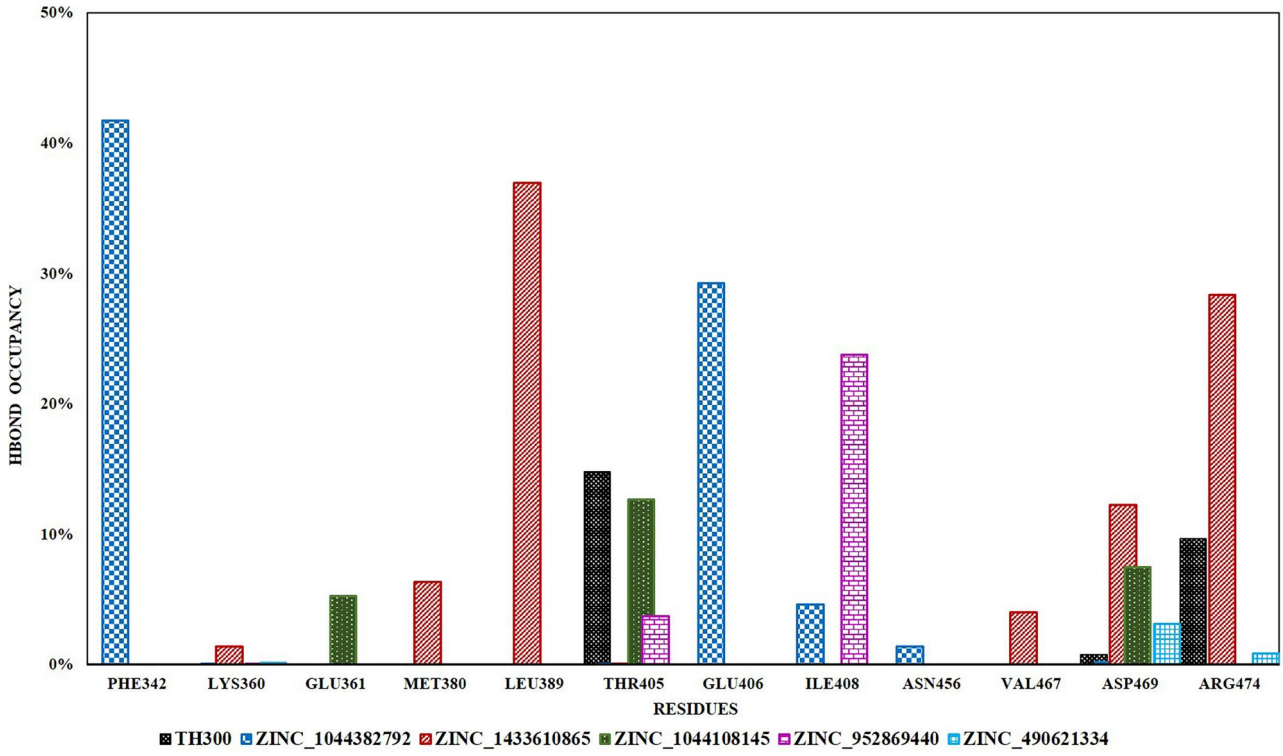

Figure 13. Comparative H-bond occupancy analysis of the LIMK2-inhibitor complexes.

Table 7. MM/PBSA calculation identified the top five compounds and determined the decomposed components of their binding free energy in units of kJ/mol.

Complexes	van der Waals energy (kJ/mol)	Electrostatic energy (kJ/mol)	Polar solvation energy (kJ/mol)	SASA energy (kJ/mol)	Binding energy (kJ/mol)
LIMK2-TH300	−248.284 ± 1.208	−38.237 ± 1.211	198.277 ± 1.277	−24.642 ± 0.085	−112.886 ± 1.593
LIMK2-ZINC1044382792	−165.443 ± 0.899	−41.478 ± 0.788	140.135 ± 1.234	−16.778 ± 0.068	−83.491 ± 1.230
LIMK2-ZINC1433610865	−168.784 ± 1.347	−14.136 ± 1.075	109.727 ± 1.626	−16.917 ± 0.071	−90.122 ± 1.248
LIMK2-ZINC1044109145	−173.075 ± 1.076	−57.762 ± 1.515	185.245 ± 2.398	−16.755 ± 0.070	−62.264 ± 1.713
LIMK2-ZINC952869440	−172.271 ± 1.239	−95.152 ± 2.091	227.843 ± 1.680	−17.413 ± 0.083	−56.957 ± 1.421
LIMK2-ZINC490621334	−172.123 ± 0.990	−34.903 ± 1.223	163.907 ± 1.609	−16.752 ± 0.069	−59.871 ± 1.395

hinge region residues have made prominent contacts only with compounds ZINC1044108145 and ZINC952869440. The crucial αC residue Met380 which has formed hydrophobic interactions with reference inhibitor TH300 was observed to have maintained higher contacts with ZINC1433610865, ZINC1044108145, and ZINC490621334.

MM/PBSA-based binding free energy calculation and decomposition analysis

From the binding free energies of the complexes (Table 7), it was observed that van der Waals energy and electrostatic energy have significantly favored the higher binding affinity of reference compound TH300. Amongst the prioritized compounds in complex with LIMK2, the LIMK2-ZINC143361086 complex (–90.122 ± 1.248 kJ/mol) followed by complex LIMK2-ZINC1044382792 (–83.491 ± 1.230 kJ/mol) has shown least binding energy with higher affinity than other compounds. Despite the increased non-bonded interactions such as van der Waals energy and electrostatic energy, due to the highly unfavoured solvation energies, the complexes LIMK2-ZINC1044109145, LIMK2-ZINC952869440, and LIMK2-ZINC490621334 has shown least binding affinity. Furthermore, the key residue that aids in the prominent binding affinity of the LIMK2 and inhibitors was observed from the per residue free energy analysis (Figure 14). In the case of the N-lobe residues, the following residues, namely, Leu337 (β1), Phe342 (g.l), Ala345 (β2), Val358, Met359, Leu362 (β3), Glu376, Met380 (αC), b.l (Leu383, Val388, Leu389, Lys390) and Phe391 (β4) have shown highly favorable interactions with the compounds. Among these residues, Glu376 (αC) and Val388 (b.l) of LIMK2 have shown unfavorable interactions with compounds ZINC1044109145 and ZINC1433610865 respectively. Additionally, it was also observed that among the conserved β sheet of LIMK2 N-lobe residues, except for Leu362 (β3) and Phe391 (β4), the other residues, namely Leu337 (β1), Ala345 (β2), Val358, Met359 (β3), have contributed significantly for the higher binding affinity of the compound ZINC1044382792 to LIMK2. Other than this, the crucial αC (Met380) and b.l (Leu383, Val388) residues have shown significant energy contributions in all complexes except for ZINC1044382792 and ZINC952869440. On analyzing the C-lobe residues, β5 (Leu403, Leu404), GK (Thr405), hinge (Tyr407), αE (Leu442), β6 (Ile447), XDFG

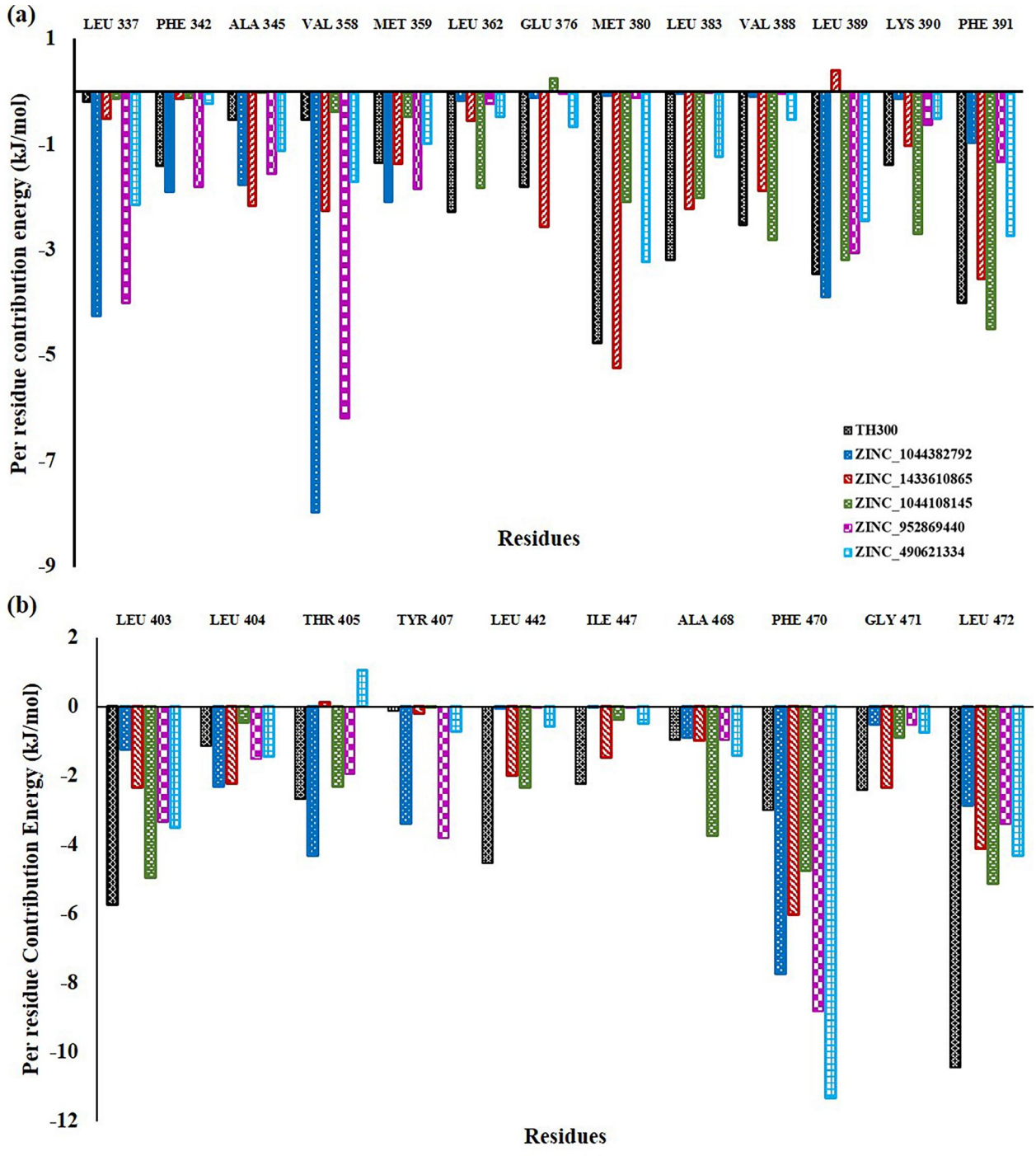

Figure 14. Per-residue free energy contributions of complexes.

(Ala468, Asp469, Phe470, Gly471), a.l (Leu472) and Arg474 were observed to be the significant contributors for increased binding affinity of the compounds to LIMK2. In these DFG motif residues (Asp469, Phe470, Gly471), Leu472, and Arg474 were observed to be the prominent residues that aided in the strong binding affinity of the complexes. Amongst the complexes studied, only the LIMK2-ZINC490621334 complex with the GK residue (Thr405) has shown unfavorable energy contribution, while the hinge residue (Tyr407) has shown negligible energy contributions in LIMK2-TH300 complex and LIMK2-ZINC1433610865 complex.

Conclusion

LIMK2 (LIM domain kinase 2) is a crucial serine/threonine protein kinase involved in fundamental cellular processes, including cell motility, cell division, and actin cytoskeleton dynamics. Its overexpression has been implicated in various malignancies, such as bladder cancer, osteosarcoma, glioblastoma, pancreatic cancer, lung cancer, and Triple Negative Breast cancer. Despite the promise of small molecule kinase inhibitors in cancer treatment, drug resistance remains a formidable obstacle, particularly with Type I inhibitors targeting the ATP-binding site, owing to limited selectivity and potential toxicity.

To tackle these challenges, our study explores the potential of Type III or allosteric inhibitors, which bind outside the ATP-binding site, aiming to achieve more effective kinase inhibition and improved clinical outcomes in oncology. Our investigation focuses on small molecule inhibitors designed to mimic Type III inhibitors, employing computational methods, including e-Pharmacophore-based High-Throughput Virtual Screening (HTVS) and molecular dynamics simulations. Through rigorous screening of the ZINC database, we have identified several compounds, notably ZINC1044382792, ZINC1433610865, ZINC1044109145, ZINC952869440, and ZINC490621334, which exhibit enhanced pharmacokinetic properties. These compounds interact with critical residues of LIMK2, including Asp469 (part of the 'DFG' motif), Leu389 (belonging to the activation loop), Phe391 (associated with β4), Thr405 (part of the G.K motif), and hinge residues (Glu406, Ile408), suggesting their potential as effective inhibitors. Comparative analysis of LIMK2-inhibitor complexes reveals that ZINC1044382792, ZINC1433610865, and ZINC490621334 exhibit remarkable stability with minimal fluctuations observed. Furthermore, the LIMK2-ZINC1433610865 and LIMK2-ZINC1044382792 complexes maintain stable hydrogen bond interactions, underscoring their favorable binding characteristics. Further investigation of binding free energies highlights that the LIMK2-ZINC1433610865 and LIMK2-ZINC1044382792 complexes possess the lowest binding energies and highest affinities compared to other compounds. Consequently, ZINC1433610865 and ZINC1044109145 emerge as promising leads for targeting LIMK2 in pathological conditions, especially cancer. Overall, our study underscores the significance of understanding allosteric inhibition and its potential advantages in overcoming challenges associated with kinase inhibitors. This research paves the way for targeted therapeutics in the treatment of human diseases, notably cancer, offering hope for improved clinical outcomes.

Disclosure statement

The authors affirm that they have no known financial or interpersonal conflicts that would have appeared to have an impact on the research presented in this study.

Funding

The authors thank TANSCHE [RGP/2019-20/ALU/HECP-0049 dated: 27/04/2021], Department of Biotechnology-Bioinformatics Centre (DBT-BIC)-No.BT/PR40154/BTIS/137/34/2021, DBT-NNP-No.BT/PR40156/BTIS/137/54/2023, DST INDO-TAIWAN (GITA/DST/TWN/P-86/2019), ST-Fund for Improvement of S &T Infrastructure in Universities Higher Educational Institutions (FIST) [SR/FST/LSI-667/2016] (C), and DST-Promotion of University Research and Scientific Excellence (PURSE phase II) (No. SR/PURSE Phase 2/38(G), 2017), MHRD-RUSA 2.0, New Delhi (F.24e51/2014-U, NH greatly acknowledges the Department of Science and Technology (DST), for financial assistance through DST/INSPIRE Fellowship/2019/IF190083.

References

Bakchi, B., Krishna, A. D., Sreecharan, E., Ganesh, V. B. J., Niharika, M., Maharshi, S., Puttagunta, S. B., Sigalapalli, D. K., Bhandare, R. R., & Shaik, A. B. (2022). An overview on applications of SwissADME web tool in the design and development of anticancer, antitubercular and antimicrobial agents: A medicinal chemist's perspective. *Journal of Molecular Structure*, *1259*, 132712. https://doi.org/10.1016/j.molstruc.2022.132712

Berabez, R., Routier, S., Bénédetti, H., Plé, K., & Vallée, B. (2022). LIM kinases, promising but reluctant therapeutic targets. chemistry and preclinical validation *in vivo*. *Cells*, *11*(13), 2090. https://doi.org/10.3390/cells11132090

Berendsen, H. J. C., Postma, J. P. M., van Gunsteren, W. F., DiNola, A., & Haak, J. R. (1984). Molecular dynamics with coupling to an external bath. *The Journal of Chemical Physics*, *81*(8), 3684–3690. https://doi.org/10.1063/1.448118

Blanc, J., Geney, R., & Menet, C. (2013). Type II kinase inhibitors. An opportunity in cancer for rational design. *Anti-Cancer Agents in Medicinal Chemistry*, *13*(5), 731–747. https://doi.org/10.2174/1871520611313050008

Bochevarov, A. D., Harder, E., Hughes, T. F., Greenwood, J. R., Braden, D. A., Philipp, D. M., Rinaldo, D., Halls, M. D., Zhang, J. [., & Friesner, R. A. (2013). Jaguar: A high-performance quantum chemistry software program with strengths in life and materials sciences. *International Journal of Quantum Chemistry*, *113*(18), 2110–2142. https://doi.org/10.1002/qua.24481

Botello-Smith, W. M., & Luo, R. (2015). Applications of MMPBSA to Membrane Proteins I: Efficient numerical solutions of periodic poisson-boltzmann equation. *Journal of Chemical Information and Modeling*, *55*(10), 2187–2199. https://doi.org/10.1021/acs.jcim.5b00341

Croft, D. R., Crighton, D., Samuel, M. S., Lourenco, F. C., Munro, J., Wood, J., Bensaad, K., Vousden, K. H., Sansom, O. J., Ryan, K. M., & Olson, M. F. (2011). p53-mediated transcriptional regulation and activation of the actin cytoskeleton regulatory RhoC to LIMK2 signaling pathway promotes cell survival. *Cell Research*, *21*(4), 666–682. https://doi.org/10.1038/cr.2010.154

Daina, A., Michielin, O., & Zoete, V. (2017). Swissadme: A free web tool to evaluate pharmacokinetics, drug-likeness and medicinal chemistry friendliness of small molecules. *Scientific Reports*, *7*(1), 42717. https://doi.org/10.1038/srep42717

Dasari, A., Sobrero, A., Yao, J., Yoshino, T., Schelman, W., Yang, Z., Chien, C., Kania, M., Tabernero, J., & Eng, C. (2021). FRESCO-2. A global Phase III study investigating the efficacy and safety of fruquintinib in metastatic colorectal cancer. *Future Oncology*, *17*(24), 3151–3162. https://doi.org/10.2217/fon-2021-0202

Dixon, S. L., Smondyrev, A. M., Knoll, E. H., Rao, S. N., Shaw, D. E., & Friesner, R. A. (2006). Phase: A new engine for pharmacophore perception, 3D QSAR model development, and 3D database screening: Methodology and preliminary results. *Journal of Computer-Aided Molecular Design*, *20*(10–11), 647–671. https://doi.org/10.1007/s10822-006-9087-6

Dixon, S. L., Smondyrev, A. M., & Rao, S. N. (2006). Phase: A novel approach to pharmacophore modeling and 3D database searching. *Chemical Biology & Drug Design*, *67*(5), 370–372. https://doi.org/10.1111/j.1747-0285.2006.00384.x

Duffy, E. M., & Jorgensen, W. L. (2000). Prediction of properties from simulations: Free energies of solvation in hexadecane, octanol, and water. *Journal of the American Chemical Society*, *122*(12), 2878–2888. https://doi.org/10.1021/ja993663t

Eswar, N., Webb, B., Marti-Renom, M. A., Madhusudhan, M. S., Eramian, D., Shen, M. -Y., Pieper, U., & Sali, A. (2006). Comparative protein structure modeling using Modeller. *Current Protocols in Bioinformatics*, *15*(1), Unit-5.6. https://doi.org/10.1002/0471250953.bi0506s15

Fasano, M., Della Corte, C. M., Califano, R., Capuano, A., Troiani, T., Martinelli, E., Ciardiello, F., & Morgillo, F. (2014). Type III or allosteric kinase inhibitors for the treatment of non-small cell lung cancer. *Expert Opinion on Investigational Drugs*, *23*(6), 809–821. https://doi.org/10.1517/13543784.2014.902934

Friesner, R. A., Banks, J. L., Murphy, R. B., Halgren, T. A., Klicic, J. J., Mainz, D. T., Repasky, M. P., Knoll, E. H., Shelley, M., Perry, J. K., Shaw, D. E., Francis, P., & Shenkin, P. S. (2004). Glide: A new approach for rapid, accurate docking and scoring. 1. Method and assessment of docking accuracy. *Journal of Medicinal Chemistry*, *47*(7), 1739–1749. https://doi.org/10.1021/jm0306430

Friesner, R. A., Murphy, R. B., Repasky, M. P., Frye, L. L., Greenwood, J. R., Halgren, T. A., Sanschagrin, P. C., & Mainz, D. T. (2006). Extra precision glide: Docking and scoring incorporating a model of hydrophobic enclosure for protein-ligand complexes. *Journal of Medicinal Chemistry*, *49*(21), 6177–6196. https://doi.org/10.1021/jm051256o

Genheden, S., & Ryde, U. (2015). The MM/PBSA and MM/GBSA methods to estimate ligand-binding affinities. *Expert Opinion on Drug Discovery*, *10*(5), 449–461. https://doi.org/10.1517/17460441.2015.1032936

Goodwin, N. C., Cianchetta, G., Burgoon, H. A., Healy, J., Mabon, R., Strobel, E. D., Allen, J., Wang, S., Hamman, B. D., & Rawlins, D. B. (2015). Discovery of a type III inhibitor of LIM kinase 2 that binds in a DFG-out conformation. *ACS Medicinal Chemistry Letters*, *6*(1), 53–57. https://doi.org/10.1021/ml500242y

Hess, B., Bekker, H., Berendsen, H. J. C., & Fraaije, J. G. E. M. (1997). LINCS. A linear constraint solver for molecular simulations. *Journal of Computational Chemistry*, *18*(12), 1463–1472. https://doi.org/10.1002/(SICI)1096-987X(199709)18:12<1463:AID-JCC4>3.0.CO;2-H

Heymach, J. V., Mitsudomi, T., Harpole, D., Aperghis, M., Jones, S., Mann, H., Fouad, T. M., & Reck, M. (2022). Design and Rationale for a Phase III, double-blind, placebo-controlled study of neoadjuvant durvalumab + chemotherapy followed by adjuvant durvalumab for the treatment of patients with resectable stages II and III non-small-cell lung cancer. The AEGEAN Trial. *Clinical Lung Cancer*, *23*(3), e247–e251. https://doi.org/10.1016/j.cllc.2021.09.010

Huang, J., Rauscher, S., Nawrocki, G., Ran, T., Feig, M., Groot, B. L. D., Grubmüller, H., & MacKerell, A. D. (2017). Charmm36m: An improved force field for folded and intrinsically disordered proteins. *Nature Methods*, *14*(1), 71–73. https://doi.org/10.1038/nmeth.4067

Jiao, Q., Bi, L., Ren, Y., Song, S., Wang, Q., & Wang, Y.-S. (2018). Advances in studies of tyrosine kinase inhibitors and their acquired resistance. *Molecular Cancer*, *17*(1), 36. https://doi.org/10.1186/s12943-018-0801-5

Jo, S., Kim, T., Iyer, V. G., & Im, W. (2008). Charmm-GUI: A web-based graphical user interface for CHARMM. *Journal of Computational Chemistry*, *29*(11), 1859–1865. https://doi.org/10.1002/jcc.20945

Jorgensen, W. L., & Duffy, E. M. (2002). Prediction of drug solubility from structure. *Advanced Drug Delivery Reviews*, *54*(3), 355–366. https://doi.org/10.1016/S0169-409X(02)00008-X

Kumari, R., Kumar, R., & Lynn, A. (2014). G_mmpbsa–a GROMACS tool for high-throughput MM-PBSA calculations. *Journal of Chemical Information and Modeling*, *54*(7), 1951–1962. https://doi.org/10.1021/ci500020m

Laskowski, R. A., MacArthur, M. W., Moss, D. S., & Thornton, J. M. (1993). PROCHECK: A program to check the stereochemical quality of protein structures. *Journal of Applied Crystallography*, *26*(2), 283–291. https://doi.org/10.1107/S0021889892009944

Lehtola, S., Dimitrova, M., Fliegl, H., & Sundholm, D. (2021). Benchmarking magnetizabilities with recent density functionals. *Journal of Chemical Theory and Computation*, *17*(3), 1457–1468. https://doi.org/10.1021/acs.jctc.0c01190

Maekawa, M., Ishizaki, T., Boku, S., Watanabe, N., Fujita, A., Iwamatsu, A., Obinata, T., Ohashi, K., Mizuno, K., & Narumiya, S. (1999). Signaling from Rho to the actin cytoskeleton through protein kinases ROCK and LIM-kinase. *Science*, *285*(5429), 895–898. https://doi.org/10.1126/science.285.5429.895

Maisuradze, G. G., Liwo, A., & Scheraga, H. A. (2009). Principal component analysis for protein folding dynamics. *Journal of Molecular Biology*, *385*(1), 312–329. https://doi.org/10.1016/j.jmb.2008.10.018

Manetti, F. (2012). LIM kinases are attractive targets with many macromolecular partners and only a few small molecule regulators. *Medicinal Research Reviews*, *32*(5), 968–998. https://doi.org/10.1002/med.20230

Mathea, S., Salah, E., Hanke, T., Newman, J. A., Oerum, S., Wang, D., Burgess-Brown, N., Delft, F. V., Arrowsmith, C. H., Edwards, A. M., Bountra, C., Bullock, A. N., & Knapp, S. (2017). *LIM Domain Kinase 2 (LIMK2) in Complex with TH-300*. https://doi.org/10.2210/pdb5NXD/pdb

Morales-Quinones, M., Ramirez-Perez, F. I., Foote, C. A., Ghiarone, T., Ferreira-Santos, L., Bloksgaard, M., Spencer, N., Kimchi, E. T., Manrique-Acevedo, C., Padilla, J., & Martinez-Lemus, L. A. (2020). LIMK (LIM Kinase) inhibition prevents vasoconstriction- and hypertension-induced arterial stiffening and remodeling. *Hypertension*, *76*(2), 393–403. https://doi.org/10.1161/HYPERTENSIONAHA.120.15203

Noureddine, O., Issaoui, N., & Al-Dossary, O. (2021). Dft and molecular docking study of chloroquine derivatives as antiviral to coronavirus COVID-19. *Journal of King Saud University. Science*, *33*(1), 101248. https://doi.org/10.1016/j.jksus.2020.101248

Okaniwa, M., Hirose, M., Imada, T., Ohashi, T., Hayashi, Y., Miyazaki, T., Arita, T., Yabuki, M., Kakoi, K., Kato, J., Takagi, T., Kawamoto, T., Yao, S., Sumita, A., Tsutsumi, S., Tottori, T., Oki, H., Sang, B.-C., Yano, J., … Ishikawa, T. (2012). Design and synthesis of novel DFG-out RAF/vascular endothelial growth factor receptor 2 (VEGFR2) inhibitors. 1. Exploration of 5,6-fused bicyclic scaffolds. *Journal of Medicinal Chemistry*, *55*(7), 3452–3478. https://doi.org/10.1021/jm300126x

Richters, A., Nguyen, H. D., Phan, T., Simard, J. R., Grütter, C., Engel, J., & Rauh, D. (2014). Identification of type II and III DDR2 inhibitors. *Journal of Medicinal Chemistry*, *57*(10), 4252–4262. https://doi.org/10.1021/jm500167q

Riyadi, P H, Sari, I D, Kurniasih, R A, Agustini, T W, Swastawati, F, Herawati, V E, Tanod, W A, Romadhon, (2021). SwissADME predictions of pharmacokinetics and drug-likeness properties of small molecules present in Spirulina platensis. *IOP Conference Series*, *890*(1),012021. https://doi.org/10.1088/1755-1315/890/1/012021

Roskoski, R. (2020). Properties of FDA-approved small molecule protein kinase inhibitors. A 2020 update. *Pharmacological Research*, *152*, 104609. https://doi.org/10.1016/j.phrs.2019.104609

Roskoski, R. (2021). Properties of FDA-approved small molecule protein kinase inhibitors. A 2021 update. *Pharmacological Research*, *165*, 105463. https://doi.org/10.1016/j.phrs.2021.105463

Roskoski, R. (2023). Properties of FDA-approved small molecule protein kinase inhibitors. A 2023 update. *Pharmacological Research*, *187*, 106552. https://doi.org/10.1016/j.phrs.2022.106552

Shahab, S., Sheikhi, M., Alnajjar, R., Saud, S. A., Khancheuski, M., & Strogova, A. (2021). Dft investigation of atazanavir as potential inhibitor for 2019-nCoV coronavirus M protease. *Journal of Molecular Structure*, *1228*, 129461. https://doi.org/10.1016/j.molstruc.2020.129461

Sooreshjani, M. A., Nikhil, K., Kamra, M., Nguyen, D. N., Kumar, D., & Shah, K. (2021). LIMK2-NKX3.1 engagement promotes castration-resistant prostate cancer. *Cancers*, *13*(10), 2324. https://doi.org/10.3390/cancers13102324

Su, Y., Xu, B., Shen, Q., Lei, Z., Zhang, W., & Hu, T. (2022). LIMK2 is a novel prognostic biomarker and correlates with tumor immune cell infiltration in lung squamous cell carcinoma. *Frontiers in Immunology*, *13*, 788375. https://doi.org/10.3389/fimmu.2022.788375

Sumi, T., Matsumoto, K., Takai, Y., & Nakamura, T. (1999). Cofilin phosphorylation and actin cytoskeletal dynamics regulated by rho- and Cdc42-activated LIM-kinase 2. *The Journal of Cell Biology*, *147*(7), 1519–1532. https://doi.org/10.1083/jcb.147.7.1519

Tuccinardi, T. (2021). What is the current value of MM/PBSA and MM/GBSA methods in drug discovery? *Expert Opinion on Drug Discovery*, *16*(11), 1233–1237. https://doi.org/10.1080/17460441.2021.1942836

Wang, C., Greene, D., Xiao, L., Qi, R., & Luo, R. (2017). Recent developments and applications of the MMPBSA Method. *Frontiers in Molecular Biosciences*, *4*, 87. https://doi.org/10.3389/fmolb.2017.00087

Wang, S., Ren, T., Jiao, G., Huang, Y., Bao, X., Zhang, F., Liu, K., Zheng, B., Sun, K., & Guo, W. (2017). BMPR2 promotes invasion and metastasis via the RhoA-ROCK-LIMK2 pathway in human osteosarcoma cells. *Oncotarget*, *8*(35), 58625–58641. https://doi.org/10.18632/oncotarget.17382

Wang, W., Yang, C., Nie, H., Qiu, X., Zhang, L., Xiao, Y., Zhou, W., Zeng, Q., Zhang, X., Wu, Y., Liu, J., & Ying, M. (2019). LIMK2 acts as an oncogene in bladder cancer and its functional SNP in the microRNA-135a binding site affects bladder cancer risk. *International Journal of Cancer*, *144*(6), 1345–1355. https://doi.org/10.1002/ijc.31757

Wu, P., Clausen, M. H., & Nielsen, T. E. (2015a). Allosteric small-molecule kinase inhibitors. *Pharmacology & Therapeutics*, *156*, 59–68. https://doi.org/10.1016/j.pharmthera.2015.10.002

Wu, P., Nielsen, T. E., & Clausen, M. H. (2015b). FDA-approved small-molecule kinase inhibitors. *Trends in Pharmacological Sciences*, *36*(7), 422–439. https://doi.org/10.1016/j.tips.2015.04.005

Yoshioka, K., Foletta, V., Bernard, O., & Itoh, K. (2003). A role for LIM kinase in cancer invasion. *Proceedings of the National Academy of Sciences of the United States of America*, *100*(12), 7247–7252. https://doi.org/10.1073/pnas.1232344100

Zhang, J., Yang, P. L., & Gray, N. S. (2009). Targeting cancer with small molecule kinase inhibitors. *Nature Reviews. Cancer*, *9*(1), 28–39. https://doi.org/10.1038/nrc2559

Zhao, Z., Wu, H., Wang, L., Liu, Y., Knapp, S., Liu, Q., & Gray, N. S. (2014). Exploration of type II binding mode. A privileged approach for kinase inhibitor focused drug discovery? *ACS Chemical Biology*, *9*(6), 1230–1241. https://doi.org/10.1021/cb500129t